



# Advanced Vibration Mitigation with Novel Stiffened Inertial Amplifier Designs

Sondipon Adhikari  and Sudip Chowdhury 

Infrastructure & Engineering, James Watt School of Engineering, The University of Glasgow, Glasgow, UK

## ABSTRACT

Inertial amplifiers are receiving increasing attention due to their superior potential for vibration attenuation under a wide range of dynamic excitations. This paper proposes and subsequently analyzes new inertial amplifier designs capable of simultaneous amplification of the effective mass and stiffness of a resonant single-degree-of-freedom dynamic system. The inertial amplifier configuration is conceived through constrained link-bar mechanisms with masses and springs attached at selected points. Three new configurations, namely the compound, nested, and levered inertial amplifiers, are introduced. The mass and stiffness amplification factors for all the amplifiers are derived in closed form by analysing the dynamics of the underlying mechanisms. Based on the analytical expressions, parameter choices for superior amplification are obtained analytically. Numerical results demonstrate that it is possible to achieve several orders of magnitude of mass and stiffness amplifications. Using the amplified effective mass and stiffness, the ability to tune the natural frequency of the inertially amplified dynamic system has been established. The inertial amplifiers proposed and designed here will deliver significantly higher effective mass and stiffness than what is used within the mechanisms. This will lead to superior passive vibration control opportunities, exploiting the ability to manipulate the resonance frequency of the underlying oscillatory system.

## ARTICLE HISTORY

Received 9 December 2024

Accepted 12 June 2025

## KEYWORDS

Stiffened inertial amplifier;  
compound inertial amplifier;  
nested inertial amplifier;  
levered inertial amplifier

## 1. Introduction

Vibration reduction in resonant structures can be achieved in two broad ways. The first approach is to enhance the damping in a structure so that the vibration amplitudes near the resonance frequencies become lower. Conceptually, this is straightforward. However, achieving higher damping requires innovation in material science involving extensive experimental testing and development. The second approach is to move or alter the natural frequencies so that they avoid resonance around dominant excitation frequencies. Vibration absorbers (Den Hartog 1985; Rivin 2003) are the most prominent examples of the second approach. This requires the ability to change the effective mass or stiffness of the system or both. The motivation of this paper lies in the second approach. It will be shown that a new class of stiffened inertial amplifiers has the capability of extreme modulation of effective inertia and stiffness properties of an oscillatory system.

Controlling the effective mass of general dynamical systems is receiving significant attention in the current research. The concept of inertial amplification has existed since the 1960s in various forms (see, for example Goodwin (1965)). Smith (2002) proposed a device concept (named an inerter) that exploited an inertial amplification. The concept used rotating flywheels, and effectively, this can be viewed as a separate element that represents a higher mass

**CONTACT** Sudip Chowdhury  [Sudip.Chowdhury@glasgow.ac.uk](mailto:Sudip.Chowdhury@glasgow.ac.uk)  Infrastructure & Engineering, James Watt School of Engineering, The University of Glasgow, Glasgow, UK

© 2025 The Author(s). Published with license by Taylor & Francis Group, LLC.

This is an Open Access article distributed under the terms of the Creative Commons Attribution License (<http://creativecommons.org/licenses/by/4.0/>), which permits unrestricted use, distribution, and reproduction in any medium, provided the original work is properly cited. The terms on which this article has been published allow the posting of the Accepted Manuscript in a repository by the author(s) or with their consent.

without actually increasing the physical mass. Initial works on inerters involved noise and vibration reduction in automobiles. Inerters have been used for vibration absorption and reduction by various authors (Chen and Hu 2019a; Di Matteo, Masnata, and Pirrotta 2019; Giaralis and Petrini 2017; Lazar, Neild, and Wagg 2014, 2016; Marian and Giaralis 2014). More recently (Marian and Giaralis 2017), inerters have been used for vibration energy harvesting. We refer to recent review papers (Kuhnert et al. 2020; Wagg 2021) for a comprehensive overview of the current and historical perspective on the use of inerters in dynamic systems.

The classical inerter (Smith 2020) used a flywheel-gear mechanism (Smith 2020). A different route to inertial enhancement is the use of an inertial amplification mechanism (Cheng et al. 2020). This is usually achieved through a link-bar mechanism (Chen and Hu 2019b) loaded with symmetric masses and a spring (Zhao et al. 2019). Like the classical inerter (Lazar, Neild, and Wagg 2014), an inertial amplifier (Frandsen et al. 2016) also delivers an increased effective mass without increasing the physical mass (De Domenico, Ricciardi, and Zhang 2020). Therefore, inertial amplifiers are mechanisms that augment the effective inertia of a system without proportionally increasing its actual mass (Acar and Yilmaz 2013). Inertial amplifiers (Taniker and Yilmaz 2017) exploit compliant mechanisms (Chowdhury, Banerjee, and Adhikari 2021). Dynamics of compliant mechanisms (Neil Sclater 2001) and their configuration study are classical topics (Howell 2001). Historically, compliant mechanisms were used to manipulate motion only. The key conceptual difference between inerter/inertial amplifiers and classical compliant mechanisms is that such mechanics are now employed to manipulate the effective inertia of a dynamical system (Cheng et al. 2020). Inertial amplifiers (Li and Li 2018) have been used for vibration absorption and attenuation (Chowdhury, Banerjee, and Adhikari 2022), low-frequency band-gap manipulation (Yilmaz, Hulbert, and Kikuchi 2007), and piezoelectric vibration energy harvesting (Adhikari and Banerjee 2022). Recently, Alotta and Failla (2021) proposed efficient damped inerter-based vibration absorbers, and Chowdhury et al. (2023) introduced inertial amplifier Tuned Mass Dampers (Chowdhury, Banerjee, and Adhikari 2023). Building on these developments, inerter and inertial amplifier-based vibration absorbers have emerged as a promising alternative, offering enhanced dynamic performance without significant mass addition (Chowdhury and Adhikari 2025b). These absorbers leverage geometrically constrained mechanisms to amplify the effective inertia (Orta and Yilmaz 2019), enabling broader frequency coverage and improved attenuation. Recent studies have demonstrated their potential for passive control applications, including base isolation (Chowdhury and Adhikari 2025a), structural resonance suppression, and energy harvesting (Chowdhury, Adhikari, and Banerjee 2025). To further enhance the performance of these vibration absorbers, optimization schemes based on the  $H_\infty$  norm have been employed to minimize the worst-case response across a specified frequency range (Den Hartog 1985). This robust control approach ensures optimal absorber tuning and broadband vibration attenuation.

From this brief review, it is clear that inertial amplifiers are of significant current interest due to their potential for vibration reduction applications. However, the conventional rhombus-shaped four-bar mechanism commonly used (see Fig. 1b for example) is somewhat restrictive as the only parameter influencing the inertial amplification is the amplifier angle. From an engineering standpoint, it will be beneficial to have alternative mechanisms giving more design freedom. Another key limitation of the conventional design paradigm is the lack of ability and emphasis on the simultaneous manipulation of effective stiffness. Novel mechanisms allowing superior control of effective inertia and stiffness properties will eventually lead to enhanced and efficient vibration control through desired natural frequency shifts.

Inspired by the ideas of inerters and inertial amplifiers, the aim of this paper is to investigate the possibility of mechanical systems capable of manipulating the effective inertia and stiffness properties of a resonant dynamic system. A key goal here is to develop unconventional designs that will simultaneously directly enhance both the mass and stiffness of a system. Therefore, we ask the following fundamental question:

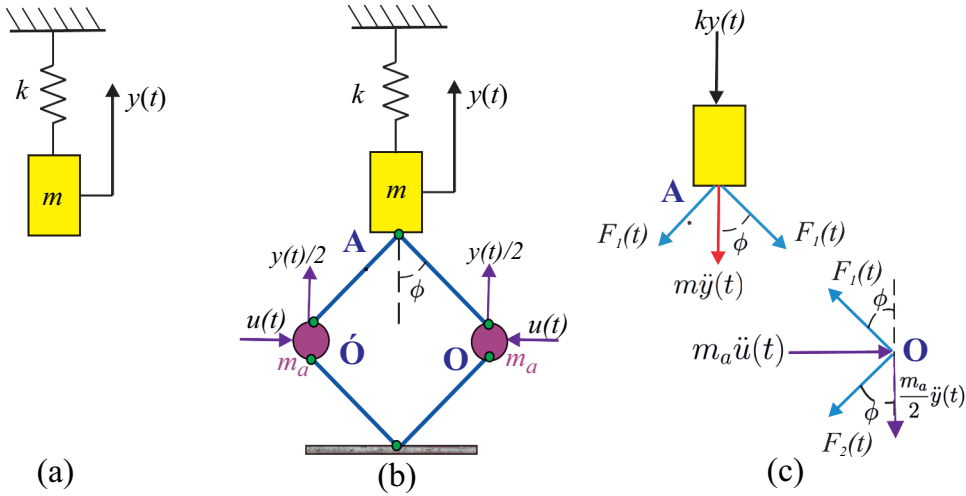


**Figure 1.** The single-degree-of-freedom (SDOF) model, the conventional inertial amplifier and the free-body diagram. (a) The mass and stiffness of the SDOF oscillator are given by  $m$  and  $k$ , respectively. (b) The conventional inertial amplifier with mass  $m_a$  and amplifier angle is  $\phi$ . The inertial amplifier is attached to an undamped spring-mass system. (c) The free-body diagram for the conventional inertial amplifier. The displacement of the mass (at point A) and the amplifier (at point O) are denoted by  $y(t)$  and  $u(t)$ , respectively. The forces  $F_1(t)$  and  $F_2(t)$  are the internal forces within the rigid links.

- In what way can masses and stiffness elements be placed within a mechanical system so that their effective mass and stiffness can be manipulated and controlled in the desired manner?

Four novel amplifier mechanisms have been proposed in this paper to address this. It will be shown that under certain design choices, it is possible to have a mechanical system with significantly greater control of the natural frequencies. These novel stiffened amplifiers are applied in the core material of the conventional base isolator to increase its vibration reduction capacity. Accordingly, four stiffened amplifier base isolators are introduced.  $H_\infty$  optimization is employed to derive the optimal design parameters of these novel isolators. The vibration reduction capacity of novel isolators is compared to the vibration reduction capacity of conventional base isolators to find their superior vibration reduction capacities.

## 2. Inertial Amplifiers

The inertial amplifiers are applied to the structures to attenuate their vibration. Three different types of novel inertial amplifiers including the conventional one are introduced in this section.

### 2.1. The Conventional Inertial Amplifier

The conventional inertial amplifier is shown in Fig. 1a.

This model has been extensively considered in recent years. Here, a brief review of it has been presented for the sake of completeness, and a comparison with other inertial amplifiers is to be introduced in the paper. The equation of motion of free vibration of the undamped SDOF oscillator in Fig. 1a is given by

$$m\ddot{y}(t) + ky(t) = 0. \quad (1)$$

A fundamental interest in this paper is how the effective mass (and the stiffness) of the system change due to the introduction of the inertial amplifier. The inertial amplifier in Fig. 1b and the others subsequently introduced in this paper are a special class of general inerters. They can be viewed as

grounded inerters with variable inertance (the effective mass). It will be rigorously shown that the variable inertance can be precisely quantified based on the mechanisms' geometric configurations (angles).

The primary mass of the single-degree-of-freedom (SDOF) oscillator and the SDOF oscillator with the inertial amplifier is exactly the same. The inertial amplifier is constructed by placing masses  $m_a$  within a rhombus mechanism made of four rigid links. The amplifier angle is  $\phi$  with respect to the vertical line, and it is assumed that the rhombus mechanism can move freely in a frictionless manner about the hinges marked in Fig. 1b by green dots. The free-body diagram for the conventional inertial amplifier is shown in Fig. 1c. The displacement of the mass (at point A) and the amplifier mass (at point O) are denoted by  $y(t)$  and  $u(t)$ , respectively. The motions  $y(t)$  and  $u(t)$  are perpendicular to each other. The forces  $F_1(t)$  and  $F_2(t)$  are the internal forces within the rigid links. Due to the symmetry of the mechanism, the dynamics at points O and O' are the same. Therefore, it is sufficient only to consider the dynamic equilibrium at one point.

The free-body diagram of the inertial amplifier is utilized to derive the governing equation of motion of the inertially amplified single-degree-of-freedom system. Newton's second law is applied at point A of the free-body diagram. Accordingly, the governing equation of motion has been derived as

$$m\ddot{y}(t) + ky(t) + 2F_1(t) \cos \phi = 0. \quad (2)$$

Here  $F_1(t)$  is the internal force within the rigid link bars in the upper half of the mechanism. The vertical motion of point O is  $y(t)/2$  due to the vertical symmetry of the mechanism. Considering the bars in Fig. 1b are rigid, using the kinematic relationship of the rigid bars, one deduces

$$\frac{y(t)}{2} \cos \phi = u(t) \sin \phi \quad \text{or} \quad u(t) = y(t) \cot \phi / 2. \quad (3)$$

It is important to note that the amplifier angle  $\phi$  is treated as a constant geometric parameter in this analysis. This assumption is justified under the small-displacement regime and rigid-body kinematics, where the structural links are idealized as non-deformable, and the joint angles remain fixed during oscillation. Consequently,  $\phi$  does not vary with the displacement  $y(t)$ , allowing a linear kinematic relationship to be used. Due to the vertical motion of the mass  $m_a$ , the internal force in the rigid link bars in the lower half of the mechanism will be different (denoted by  $F_2(t)$ ). Recalling that the vertical motion at point O is  $y(t)/2$ , balancing the force in the vertical direction, the inertial forces are derived as

$$F_1(t) \cos \phi = F_2(t) \cos \phi + \frac{m_a}{2} \ddot{y}(t) \quad \text{or} \quad F_1(t) - F_2(t) = \frac{\frac{m_a}{2} \ddot{y}(t)}{\cos \phi}. \quad (4)$$

From the equilibrium of forces in the horizontal direction at point O one obtains

$$F_1(t) \sin \phi + F_2(t) \sin \phi = m_a \ddot{u}(t). \quad (5)$$

Using the kinematic relationship in Eq. (3) in the above equation, one deduces

$$F_1(t) + F_2(t) = \frac{1}{2} m_a \ddot{y}(t) \frac{\cot \phi}{\sin \phi}. \quad (6)$$

Adding Eqs. (4) and (6), the total inertial forces are derived as

$$2F_1(t) = \frac{1}{2} m_a \ddot{y}(t) \frac{\cot \phi}{\sin \phi} + \frac{m_a}{2} \ddot{y}(t) \frac{1}{\cos \phi}. \quad (7)$$

Substituting Eq. (7) in Eq. (2), the governing equation of motion has been derived as

$$\underbrace{\left(m + \frac{m_a}{2}(1 + \cot^2 \phi)\right)}_{m_{\text{eff}}} \ddot{y}(t) + ky(t) = 0. \quad (8)$$

The effective mass of the amplified system in Fig. 1b is  $\left(m + \frac{m_a}{2}(1 + \cot^2 \phi)\right)$ . The above equation can be rewritten as

$$m(1 + \gamma_m(1 + \cot^2 \phi)/2) \ddot{y}(t) + ky(t) = 0. \quad (9)$$

where the mass ratio is given by

$$\gamma_m = \frac{m_a}{m}. \quad (10)$$

The non-dimensional inertial amplification factor is introduced and defined as the ratio of the effective mass of the inertially amplified system to the original system as

$$\Gamma_1 = \frac{m_{\text{eff}}}{m} = 1 + \gamma_m(1 + \cot^2 \phi)/2. \quad (11)$$

This definition of the inertial amplification factor will be used to quantify the efficacy of different inertial amplifier designs proposed here.

In Fig. 2, the inertial amplification factor is plotted as a function of the amplifier angle  $\phi$ .

This is a log-plot, and it has been observed that the inertial amplification increases exponentially when the amplifier angle  $\phi$  is closer to zero. This result shows that the theoretical inertial amplification can be over 100. The two key assumptions made in deriving the equation of motion are: (1) the hinge movements between the four link-bars, the mass and the ground are frictionless, and (2) the masses of the four link-bars are negligible. When the amplifier angle  $\phi$  becomes close to zero, the mechanism becomes extremely narrow, and even very small friction in the hinges will prevent it from operating properly. Keeping this in mind, it is preferable that  $\phi \geq 10^\circ$ . This will ensure that the assumptions made are applicable to our model. Another point

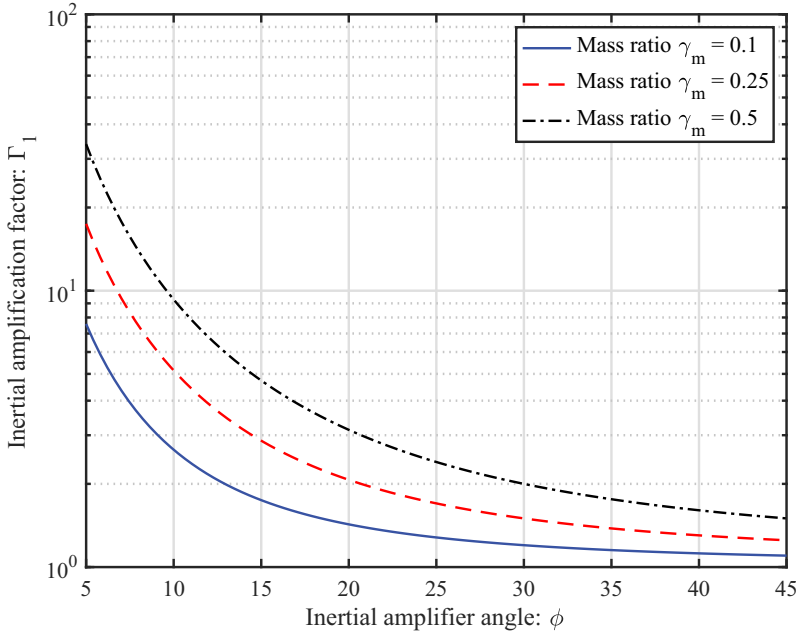


**Figure 2.** Inertial amplification as a function of the amplifier angle  $\phi$  for the conventional inertial amplifier. Three values of the mass factor  $\gamma_m$  are shown in the plot. For smaller amplifier angles  $\phi \lesssim 15^\circ$ , the inertial amplification becomes prominent.

to be noted is that the inertial amplifier effectively does not provide significant amplification when  $\phi > 45^\circ$ . Therefore, the amplifier angle should be chosen to be smaller than  $45^\circ$ . Now, the compound inertial amplifiers and their design with exact closed-form expressions are introduced.

## 2.2. The Compound Inertial Amplifier

The conventional inertial amplifier has been discussed in the previous section which has the potential for enhanced effective inertia. Now, the compound inertial amplifiers are introduced to enhance more inertial amplification. The main idea is to have multiple smaller inertial amplifiers working in unison. The proposed design of a compound inertial amplifier with two cells is shown in Fig. 3.

Two secondary mechanisms are inserted within a primary mechanism. From a practical standpoint, the outer and inner mechanisms can be placed in offset vertical planes so that their movements do not intersect each other. The primary amplifier angle is  $\phi$ , and the secondary amplifier angle is  $\theta$ . Each mass within the cells is  $m_a/2$ , so the total mass in each half is  $m_a$ , as in the case of the conventional inertial amplifier discussed in the previous section. This way, the inertial amplification performance can be compared consistently across different designs.

The displacement of the main mass (at point A), point O, and the amplifier mass (at point B) are  $y(t)$ ,  $u(t)$ , and  $v(t)$ , respectively. From Fig. 3a, observe that point D is fixed and point C only moves in the vertical direction due to the symmetry of the system. Therefore, the vertical motion at point O is

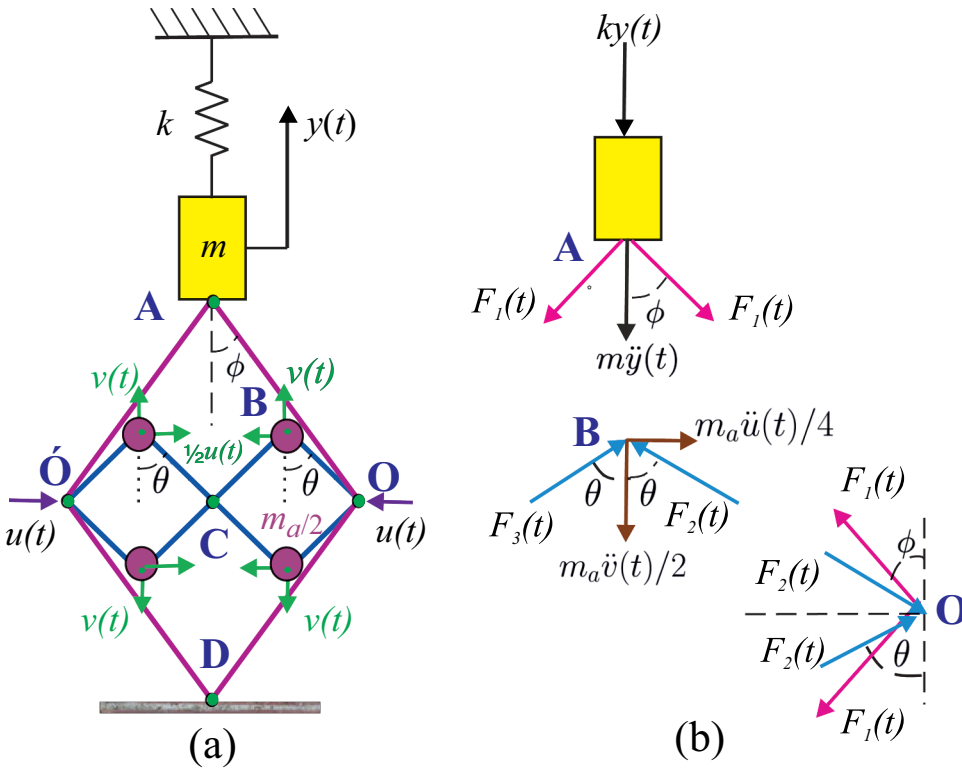


**Figure 3.** The compound inertial amplifier and its corresponding free-body diagram. (a) a compound inertial amplifier with two cells. The primary amplifier angle is  $\phi$ , and the secondary amplifier angle is  $\theta$ . Each mass within the cells is  $m_a/2$  so that the total mass is the same as the conventional inertial amplifier. (b) The free-body diagram for the compound inertial amplifier. The displacement of the mass (at point A), point O, and the amplifier mass (at point B) are denoted by  $y(t)$ ,  $u(t)$  and  $v(t)$ , respectively. The forces  $F_1(t)$ ,  $F_2(t)$  and  $F_3(t)$  are the internal forces within the rigid links of the primary and secondary mechanisms.

$y(t)/2$ , and the horizontal motion at point B is  $u(t)/2$ . Considering the bars in Fig. 3a are rigid, using the kinematic relationship of the primary mechanism, one obtains

$$\frac{y(t)}{2} \cos \phi = u(t) \sin \phi \quad \text{or} \quad u(t) = y(t) \cot \phi / 2. \quad (12)$$

From the kinematic relationship of the secondary mechanisms, the deflections in the horizontal and vertical directions are derived as

$$v(t) \cos \theta = \frac{u(t)}{2} \sin \theta \quad \text{or} \quad v(t) = u(t) \tan \theta / 2. \quad (13)$$

Combining the preceding two equations, the vertical motion of the amplifier mass  $m_a/2$  can be related to the motion of the primary mass as

$$v(t) = \frac{y(t)}{4} \cot \phi \tan \theta. \quad (14)$$

Considering the equilibrium of the forces in the vertical direction, from point B in the free-body diagram in Fig. 3b, the inertial forces are derived as

$$F_2(t) \cos \theta + F_3(t) \cos \theta = \frac{m_a}{2} \ddot{v}(t) \quad \text{or} \quad F_2(t) + F_3(t) = \frac{m_a \ddot{v}(t)/2}{\cos \theta}. \quad (15)$$

From the equilibrium of forces in the horizontal direction at point B, one obtains

$$F_3(t) \sin \theta + \frac{m_a}{4} \ddot{u}(t) = F_2(t) \sin \theta \quad \text{or} \quad F_2(t) - F_3(t) = \frac{m_a \ddot{u}(t)/4}{\sin \theta}. \quad (16)$$

Eliminating  $F_3(t)$  from the above equations the expression of  $F_2(t)$  can be obtained as

$$2F_2(t) = \frac{m_a \ddot{v}(t)}{2 \cos \theta} + \frac{m_a \ddot{u}(t)}{4 \sin \theta} = \frac{m_a}{4} \left( \frac{\tan \theta}{\cos \theta} + \frac{1}{\sin \theta} \right) \ddot{u}(t). \quad (17)$$

Using the expression of  $u(t)$  from Eq. (12), the total inertial forces at point “O” are derived as

$$2F_2(t) = \frac{m_a}{8} \cot \phi \left( \frac{\tan \theta}{\cos \theta} + \frac{1}{\sin \theta} \right) \ddot{y}(t). \quad (18)$$

Considering the equilibrium of the forces in the horizontal direction from point O in the free-body diagram, the total inertial forces have been derived as

$$2F_1(t) \sin \phi = 2F_2(t) \sin \theta \quad (19)$$

$$\text{or} \quad 2F_1(t) \cos \phi = 2F_2(t) \sin \theta \cot \phi = \frac{m_a}{8} \cot^2 \phi (1 + \tan^2 \theta) \ddot{y}(t). \quad (20)$$

Considering the equilibrium of the main mass, from point A in the free-body diagram, one has

$$m \ddot{y}(t) + ky(t) + 2F_1(t) \cos \phi = 0. \quad (21)$$

Substituting the expression of  $2F_1(t) \cos \phi$  from Eq. (20) into the above equation, the equation of motion of an SDOF oscillator with the compound inertial amplifier has been derived as

$$\underbrace{\left( m + \frac{m_a}{8} \cot^2 \phi (1 + \tan^2 \theta) \right)}_{m_{\text{eff}}} \ddot{y}(t) + ky(t) = 0. \quad (22)$$

The effective mass of the amplified system in Fig. 3a is derived as  $(m + \frac{m_a}{8} \cot^2 \phi (1 + \tan^2 \theta))$ . The non-dimensional inertial amplification factor for the compound inertial amplifier has been derived and defined as the ratio of the effective mass of the compound inertial amplifier to the original system.

$$\Gamma_2 = \frac{m_{\text{eff}}}{m} = 1 + \gamma_m (\cot^2 \phi (1 + \tan^2 \theta)) / 8. \quad (23)$$

Here, the subscript “2” is used to denote that the amplification factor is for the compound amplifier and differentiate it from the conventional amplifier given in Eq. (11).

Comparing  $\Gamma_2$  from Eq. (23) to the inertial amplification factor of the conventional amplifier in Eq. (11), the condition for the compound amplifier to outperform the conventional amplifier can be obtained as  $\Gamma_2 > \Gamma_1$ . Using the respective expressions, this translates to

$$(\cot^2 \phi (1 + \tan^2 \theta)) / 8 > (1 + \cot^2 \phi) / 2. \quad (24)$$

From this, the required condition for the secondary amplifier angle  $\theta$  can be obtained as

$$\tan^2 \theta > (3 + 4 \tan^2 \phi) \quad \text{or} \quad 2 \cos \theta < \cos \phi. \quad (25)$$

This requirement is in addition to  $\phi < 45^\circ$  required for inertial amplification from the conventional amplifier as the primary amplifier angle is normally chosen small,  $\tan^2 \phi > 0$ .

Therefore, the minimum value of  $\theta$  necessary for the compound amplifier to outperform the conventional amplifier is

$$\tan \theta > \sqrt{3} \quad \text{or} \quad \theta > 60^\circ. \quad (26)$$

To absolutely ensure the enhanced amplification of the compound amplifier, it has been considered that the limiting case when the primary amplifier angle  $\phi = 45^\circ$ . For this case, the requirement on  $\theta$  obtained from Eq. (25) as

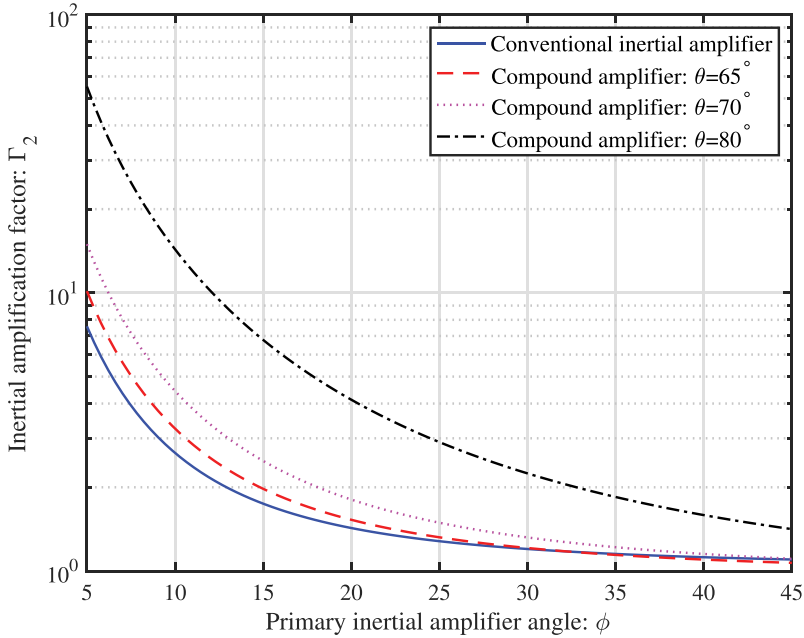


**Figure 4.** Inertial amplification as a function of the primary amplifier angle  $\phi$  for the compound amplifier SDOF system for various secondary amplifier angle  $\theta$ . The value of the mass factor  $\gamma_m = 0.1$ .



$$\tan \theta > \sqrt{7} \quad \text{or} \quad \theta \approx 70^\circ. \quad (27)$$

Using different combinations of  $\theta$  and  $\phi$ , the compound amplifier gives a wide range of design choices to suit practical applications.

In Fig. 4, the inertial amplification factor of the compound amplifier is compared for different parameter values. Amplifications for three different values of the secondary amplifier angle  $\theta$  are shown in the figure. This clearly shows that when  $\theta > 70^\circ$ , the amplification of the compound amplifier is more than its conventional counterpart. The results in Fig. 4 also give another interesting possibility which is not available for the conventional amplifier. For a given target inertial amplification, say 50, a range of combinations of  $\phi$  and  $\theta$  can be selected. This gives more opportunities for the design and satisfies any practical constraints.

### 2.3. The Nested Inertial Amplifier

In the previous section, it has been showed that inertial amplification can be enhanced by introducing secondary mechanisms within the primary mechanism. Motivated by this, here it has been taken that this idea is further in the form of a nested inertial amplifier design shown in Fig. 5.

The amplifier is obtained by introducing two connected four-bar rhombus mechanisms inside the primary mechanism. The overall design conceived in Fig. 5 is therefore made of three mechanisms, and they are marked on the figure. The amplifier mass  $m_a$  is placed inside the innermost mechanism. Therefore, the amount of amplifier mass employed is the same as in the previous two cases. The outer

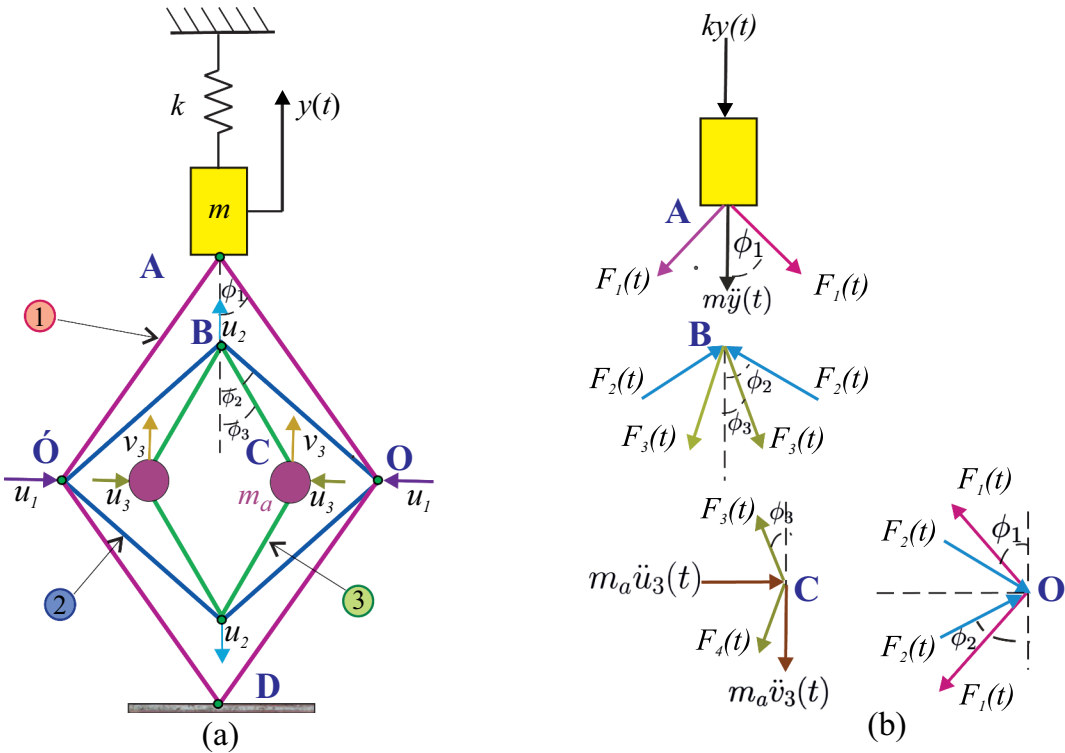


**Figure 5.** The nested inertial amplifier and its corresponding free-body diagram. (a) The nested inertial amplifier is made of three connected mechanisms. The mass  $m_a$  is placed inside the innermost mechanism. The amplifier angles for the mechanisms are  $\phi_1, \phi_2$ , and  $\phi_3$  as shown. (b) The free-body diagram for the nested inertial amplifier. The displacement of the mass (at point A), points O, B and C are denoted by  $y(t), u_1(t), u_2(t)$ , and  $u_3(t)$ , respectively. The forces  $F_i(t), i = 1, \dots, 4$  are the internal forces within the rigid links of the mechanism 1, 2, and 3, respectively.

and both inner mechanisms can be placed in offset vertical planes so that their movements do not intersect each other.

The amplifier angles for the mechanisms are  $\phi_1$ ,  $\phi_2$  and  $\phi_3$ . The displacement of the mass (at point A), points O, B, and C are  $y(t)$ ,  $u_1(t)$ ,  $u_2(t)$ , and  $u_3(t)$ , respectively. From Fig. 5a observe that point D is fixed and point B only moves in the vertical direction due to the symmetry of the system. Therefore, the vertical motion at point O is  $y(t)/2$ . Using the kinematic relationship of mechanism 1, the deflections have been obtained as

$$\frac{y(t)}{2} \cos \phi_1 = u_1(t) \sin \phi_1 \quad \text{or} \quad u_1(t) = y(t) \cot \phi_1 / 2. \quad (28)$$

Next, the motion of mechanism two is considered. Considering, for example, that the member OB is of fixed length and the deflection has been derived as

$$u_1 \sin \phi_2 = u_2 \cos \phi_2. \quad (29)$$

Finally, considering the motion of mechanism 3 and noting that the member CB is of fixed length, the expression for deflection has been obtained as

$$u_3 \sin \phi_3 = u_2 \cos \phi_3. \quad (30)$$

Combining the above three kinematic relationships, the horizontal motion of the innermost mechanism containing the mass  $m_a$  can be linked with the motion of the primary oscillating mass as

$$u_3 = \frac{y(t)}{2} \cot \phi_1 \tan \phi_2 \cot \phi_3. \quad (31)$$

For the vertical motion of the mass  $m_a$ , from point C, the deflection has been obtained as

$$v_3 \cos \phi_3 = u_3 \sin \phi_3. \quad (32)$$

Now, the free-body diagram Fig. 5b has been considered and investigated the equilibrium at various points to obtain the equation of motion. Considering the equilibrium of the main mass from point A in the free-body diagram, the governing equation of motion has been derived as

$$m\ddot{y}(t) + ky(t) + 2F_1(t) \cos \phi_1 = 0. \quad (33)$$

Recalling that the vertical motion at point C is  $y(t)/2$ , balancing the force in the vertical direction at this point, the inertial forces are derived as

$$F_3(t) \cos \phi_3 = F_4(t) \cos \phi_3 + m_a \ddot{v}_3(t) \quad \text{or} \quad F_3(t) - F_4(t) = \frac{m_a \ddot{v}_3(t)}{\cos \phi_3}. \quad (34)$$

From the equilibrium of forces in the horizontal direction at point C, one obtains

$$F_3(t) \sin \phi_3 + F_4(t) \sin \phi_3 = m_a \ddot{u}_3(t) \quad \text{or} \quad F_3(t) + F_4(t) = \frac{m_a \ddot{u}_3(t)}{\sin \phi_3}. \quad (35)$$

Adding Eqs. (34) and (35), the inertial forces are derived as

$$2F_3(t) = \frac{m_a \ddot{v}_3(t)}{\cos \phi_3} + \frac{m_a \ddot{u}_3(t)}{\sin \phi_3}. \quad (36)$$

From the equilibrium of the forces in the vertical direction, from point B in the free-body diagram, one obtains

$$2F_2 \cos \phi_2 = 2F_3 \cos \phi_3. \quad (37)$$

Considering the equilibrium of the forces in the horizontal direction from point O in the free-body diagram, the inertial forces are derived as

$$2F_1(t) \sin \phi_1 = 2F_2(t) \sin \phi_2. \quad (38)$$

Combining Eqs. (32)–(38), one can deduce

$$\begin{aligned} 2F_1(t) \cos \phi_1 &= 2F_3(t) \cos \phi_3 \tan \phi_2 \cot \phi_1 \\ &= (m_a \ddot{v}_3(t) + m_a \ddot{u}_3(t) \cot \phi_3) \tan \phi_2 \cot \phi_1 \\ &= m_a \ddot{u}_3(t) (\tan \phi_3 + \cot \phi_3) \tan \phi_2 \cot \phi_1. \end{aligned} \quad (39)$$

Now, using the expression of  $u_3$  from Eq. (31) and substituting this in Eq. (33), the equation of motion of an SDOF oscillator with the nested inertial amplifier is obtained as

$$\underbrace{\left( m + \frac{m_a}{2} (1 + \cot^2 \phi_3) \cot^2 \phi_1 \tan^2 \phi_2 \right)}_{m_{\text{eff}}} \ddot{y}(t) + ky(t) = 0. \quad (40)$$

The effective mass of the amplified SDOF oscillator in Fig. 5a is therefore given by  $\left( m + \frac{m_a}{2} (1 + \cot^2 \phi_3) \cot^2 \phi_1 \tan^2 \phi_2 \right)$ .

The non-dimensional inertial amplification factor has been derived and defined as the ratio of the effective mass of the nested inertial amplifier to the original system.

$$\Gamma_3 = \frac{m_{\text{eff}}}{m} = 1 + \gamma_m (1 + \cot^2 \phi_3) \cot^2 \phi_1 \tan^2 \phi_2 / 2. \quad (41)$$

Comparing  $\Gamma_3$  from Eq. (41) to the inertial amplification factor of the conventional amplifier in Eq. (11), the condition for the nested amplifier to outperform the conventional amplifier can be obtained as  $\Gamma_3 > \Gamma_1$ . Using the respective expressions (using the notation  $\phi = \phi_1$  for the conventional amplifier), this translates to

$$(1 + \cot^2 \phi_3) \cot^2 \phi_1 \tan^2 \phi_2 > (1 + \cot^2 \phi_1). \quad (42)$$

From this, the required condition for the amplifier angles  $\phi_2$  and  $\phi_3$  can be obtained as

$$(1 + \cot^2 \phi_3) \tan^2 \phi_2 > (1 + \tan^2 \phi_1). \quad (43)$$

As the primary amplifier angle is normally chosen small,  $\tan^2 \phi_1 \approx 0$ . Therefore, the values of  $\phi_2$  and  $\phi_3$ , which are sufficient for the nested amplifier to outperform the conventional amplifier, are

$$\tan \phi_2 > 1 \quad \text{or} \quad \phi_2 > 45^\circ \quad \text{and} \quad \cot \phi_3 > 1 \quad \text{or} \quad \phi_3 < 45^\circ. \quad (44)$$

These requirements are in addition to  $\phi_1 < 45^\circ$  required for inertial amplification from the conventional amplifier.

In Fig. 6, the inertial amplification factor of the nested amplifier is compared for different parameter values.

Amplifications for three different values of combinations of the angles  $\phi_2$  and  $\phi_3$  are shown. These results clearly show that when  $\phi_2 > 45^\circ$  and  $\phi_3 < 45^\circ$ , the amplification of the nested amplifier is much more than its conventional counterpart. The results in Fig. 6 also give another interesting possibility which is not available for the conventional amplifier. For a given target inertial amplification, say 50, a range of combinations of  $\phi_1$ ,  $\phi_2$ , and  $\phi_3$  can be selected. This gives more opportunity for the design to satisfy any practical constraints.

Comparing Figs. 6 with 4 it can be observed that the nested amplifier, in general, results in more amplification compared to the compound amplifier. This happens when

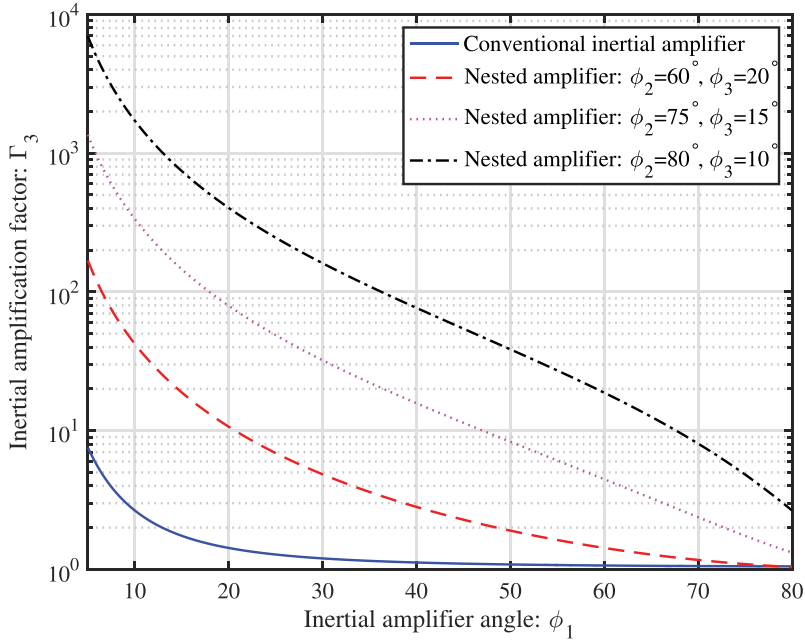


**Figure 6.** Inertial amplification as a function of the amplifier angle  $\phi_1$  for the nested amplifier SDOF system for various combinations of  $\phi_2$  and  $\phi_3$ ,  $\gamma_m = 0.1$ . The value of the mass factor undefined.

$$\begin{aligned} \Gamma_3 > \Gamma_2 \quad \text{or} \quad (1 + \cot^2 \phi_3) \cot^2 \phi_1 \tan^2 \phi_2 > (\cot^2 \phi_1 (1 + \tan^2 \theta)) / 8, \\ \text{or} \quad 2 \cos \theta < \cot \phi_2 \sin \phi_3. \end{aligned} \quad (45)$$

In the previous section, it was derived that the minimum value of  $\theta$  for the compound amplifier is  $60^\circ$ . Using the  $\theta = 60^\circ$ , the above condition becomes

$$\cot \phi_2 \sin \phi_3 > 1. \quad (46)$$

This requirement is consistent with what was derived in Eq. (44). From these discussions, it has been observed that it is possible to obtain physically realistic parameters such that the inertial amplification of the three amplifier configurations satisfies the following inequality

$$\Gamma_3 \geq \Gamma_2 \geq \Gamma_1. \quad (47)$$

This justifies the three rhombus-shaped inertial amplifier designs.

In principle, one can add more internal and nested mechanisms following the idea proposed in Figs. 3 and 5. The inertial amplification factors for such higher-order compound and nested amplifiers will be more and will follow the same trend as derived in Eqs. (23) and (41). However, care should be taken for practical consideration as there will be many moving parts in higher-order mechanisms.

## 2.4. The Levered Inertial Amplifier

So far, the three inertial amplifiers proposed all exploit rhombus-shaped four link-bar mechanisms in a novel manner. Although they are very compact and represent a space-saving design, there are many moving parts. The aim here is to conceive an amplifier design that uses relatively simpler mechanisms. The concept of an inertial amplifier that uses only mechanical levers is shown in Fig. 7.

The mass  $m_a$  is connected with the second lever arm at point O. The rods AC, CD, and DO are assumed to be rigid. In addition, the rod AC pivots freely about  $P_1$ , and the rod DO pivots freely about

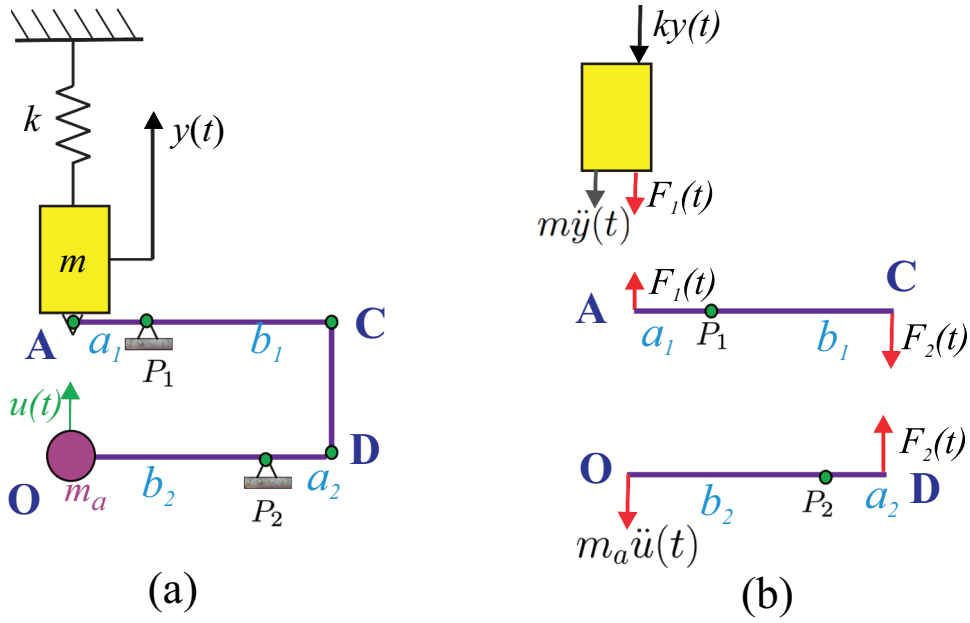


**Figure 7.** (a) The levered inertial amplifier is made of three connected rigid levers. The mass  $m_a$  is connected with the lever arm at point O. The lever arms can freely pivot about the points  $P_1$  and  $P_2$ . (b) The free-body diagram for the levered inertial amplifier. The displacement of the mass (at point A) and the amplifier (at point O) are denoted by  $y(t)$  and  $u(t)$ , respectively. The forces  $F_1(t)$  and  $F_2(t)$  are the internal forces within the rigid links.

$P_2$ . The rod CD simply connects rods AC and DO and transfers the motion and forces. Considering these, the motion at point O can be obtained as

$$u(t) = \frac{b_1 b_2}{a_1 a_2} y(t). \quad (48)$$

Now, the free-body diagram is shown in Fig. 7b and investigates the equilibrium at various points to obtain the equation of motion. Considering the equilibrium of the main mass from point A in the free-body diagram, the governing equations of motion have been derived as

$$m\ddot{y}(t) + ky(t) + F_1(t) = 0. \quad (49)$$

The rigid link AC rotates about the pivot point  $P_1$ . Therefore, taking a moment about  $P_1$ , the inertial forces have been derived as

$$F_1(t)a_1 = F_2(t)b_1. \quad (50)$$

Similarly, taking member about  $P_2$  for the rigid link OD one has

$$F_2(t)a_2 = m_a \ddot{u}(t)b_2. \quad (51)$$

Elimination of  $F_2(t)$  from the two preceding equations leads to

$$F_1(t) = m_a \ddot{u}(t) \frac{b_1 b_2}{a_1 a_2}. \quad (52)$$

Using the expression of  $u(t)$  from Eq. (48) and substituting in the equilibrium Eq. (49), the equation of motion of an SDOF oscillator with the levered inertial amplifier is obtained as

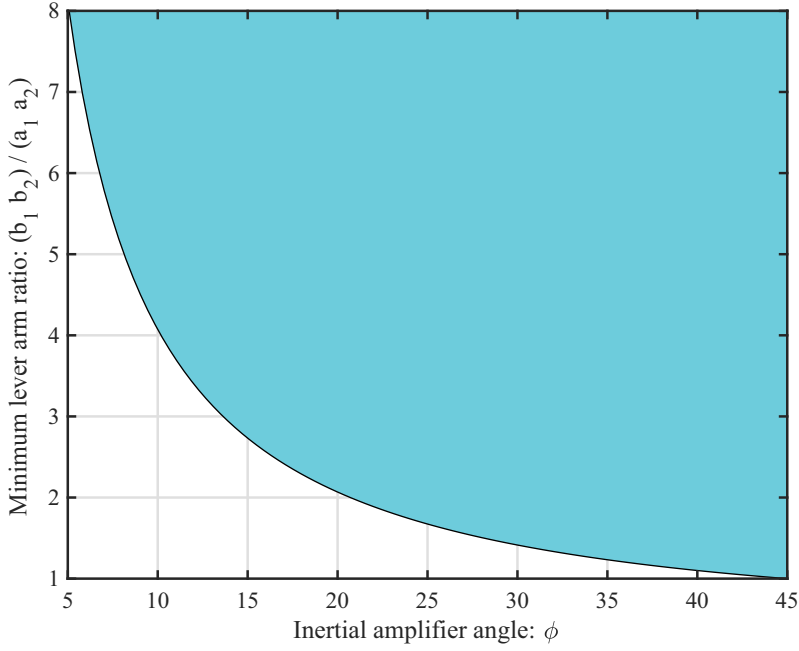


**Figure 8.** The minimum lever arm ratio necessary for the levered inertial amplifier to outperform the conventional inertial amplifier is shown as a function of the amplifier angle  $\phi$ .

$$\underbrace{\left( m + m_a \left( \frac{b_1 b_2}{a_1 a_2} \right)^2 \right)}_{m_{\text{eff}}} \ddot{y}(t) + ky(t) = 0. \quad (53)$$

The effective mass of the amplified SDOF oscillator in Fig. 7a is therefore given by  $\left( m + m_a \left( \frac{b_1 b_2}{a_1 a_2} \right)^2 \right)$ .

The non-dimensional inertial amplification factor has been derived and defined as the ratio of the effective mass of the levered inertial amplifier to the original system.

$$\Gamma_4 = \frac{m_{\text{eff}}}{m} = 1 + \gamma_m \left( \frac{b_1 b_2}{a_1 a_2} \right)^2. \quad (54)$$

Therefore, provided  $b_1 > a_1$  and  $b_2 > a_2$ , the levered amplifier in Fig. 7 will deliver an increased amplification. As an example, when  $b_1/a_1 = 4$  and  $b_2/a_2 = 3$ , the inertial amplification factor will be 144 for the levered amplifier. Comparing  $\Gamma_4$  from Eq. (54) to the inertial amplification factor of the conventional amplifier in Eq. (11), the condition for the nested amplifier to outperform the conventional amplifier can be obtained as  $\Gamma_4 > \Gamma_1$ . Using the respective expressions, this translates to

$$\left( \frac{b_1 b_2}{a_1 a_2} \right)^2 > (1 + \cot^2 \phi)/2. \quad (55)$$

From this, the required condition for the lever arm ratios are obtained as

$$\frac{b_1}{a_1} \frac{b_2}{a_2} > \frac{1}{\sqrt{2}} \operatorname{cosec} \phi. \quad (56)$$

Note that this is independent of the mass ratio of  $\gamma_m$ . To understand this requirement, in Fig. 8 the minimum lever arm ratio necessary for the levered inertial amplifier to outperform the conventional inertial amplifier is shown as a function of the amplifier angle  $\phi$ .

The shaded area shows the region of lever arm ratio, which will give more inertial amplification compared to conventional inertial amplifier for a selected value of  $\phi$ . For example, if  $\phi = 10^\circ$ , choosing lever arm ratios  $\frac{b_1}{a_1} = \frac{b_2}{a_2} = 2$  will be enough.

### 3. Stiffened Inertial Amplifiers

In the previous section, the inertial amplifier designs only employed discrete masses. This has an impact on the effective mass of the dynamic system only. If stiffness elements are used within the inertial amplifiers, it will alter the effective stiffness also. Therefore, by simultaneously using mass and stiffness elements, one can alter the effective mass and stiffness of the SDOF system. This, in turn, will make it possible to tune the resonance frequency of the oscillator using the stiffened inertial amplifier. Here, the four inertial amplifier designs proposed in the previous section are augmented using suitably placed stiffness elements. Stiffened inertial amplifiers introduced in this section can be viewed as grounded parallel inerter-spring configurations with variable inertance and stiffness. It will be rigorously shown that both the variable inertance and stiffness can be precisely quantified based on the mechanisms' geometric configurations (angles).

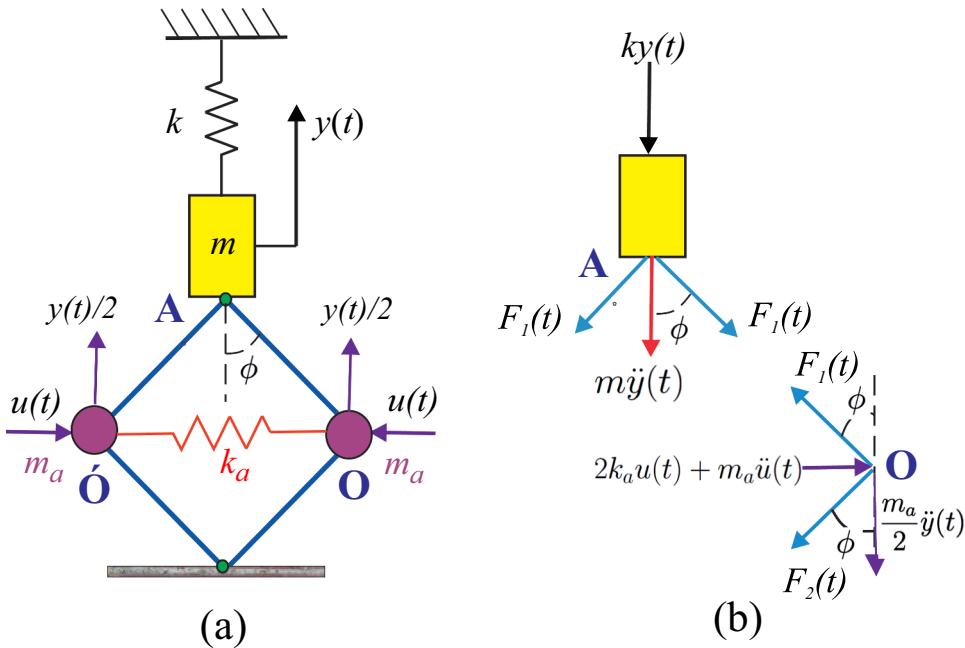


**Figure 9.** The stiffened inertial amplifier and the free-body diagram. (a) The stiffened inertial amplifier with mass  $m_a$ , stiffness  $k_a$  and the amplifier angle is  $\phi$ . The stiffened inertial amplifier is attached to an undamped spring-mass dynamic system. (b) The free-body diagram for the stiffened inertial amplifier.

### 3.1. The Stiffened Inertial Amplifier

The stiffened inertial amplifier is shown in Fig. 9.

To obtain the equation of motion, considering the equilibrium of the mass  $m$ , from point A in the free-body diagram in Fig. 9b, the governing equation of motion has been derived as

$$m\ddot{y}(t) + ky(t) + 2F_1(t) \cos \phi = 0. \quad (57)$$

Here  $F_1(t)$  is the internal force within the rigid link bars in the upper half of the mechanism. This can be obtained following the similar procedure outlined in section 3 for the case of the pure inertial amplifier. The main difference arises from the equilibrium of forces in the horizontal direction at point O. Considering this, the inertial forces are derived as

$$F_1(t) \sin \phi + F_2(t) \sin \phi = m_a \ddot{u}(t) + k_a u(t) \quad \text{or} \quad F_1(t) + F_2(t) = \frac{m_a \ddot{u}(t) + 2k_a u(t)}{\sin \phi}. \quad (58)$$

Factor 2 in the above equation arises because the spring  $k_a$  is stretched by  $2u(t)$ . Adding this with Eq. (4) the expression of  $F_1(t)$  can be obtained as

$$2F_1(t) = \frac{m_a \ddot{u}(t) + 2k_a u(t)}{\sin \phi} + \frac{m_a}{2} \ddot{y}(t) \frac{1}{\cos \phi}. \quad (59)$$

Using the expression of  $u(t)$  from the kinematic relationship in (3) in the above equation, one deduces

$$2F_1(t) = \frac{1}{2} (m_a \ddot{y}(t) + 2k_a y(t)) \frac{\cot \phi}{\sin \phi} + \frac{m_a}{2} \ddot{y}(t) \frac{1}{\cos \phi}. \quad (60)$$

Substituting this in Eq. (57), the equation of motion has been derived as

$$\underbrace{\left(m + \frac{m_a}{2} (1 + \cot^2 \phi)\right)}_{m_{\text{eff}}} \ddot{y}(t) + \underbrace{(k + k_a \cot^2 \phi)}_{k_{\text{eff}}} y(t) = 0. \quad (61)$$

The effective stiffness of the amplified system in Fig. 9 is  $(k + k_a \cot^2 \phi)$ . The above equation can be rewritten as

$$m(1 + \gamma_m (1 + \cot^2 \phi)/2) \ddot{y}(t) + k(1 + \gamma_k \cot^2 \phi) y(t) = 0. \quad (62)$$

where the stiffness ratio is given by

$$\gamma_k = \frac{k_a}{k}. \quad (63)$$

The non-dimensional stiffness amplification factor is derived and defined as the ratio of the effective stiffness of the inertially amplified system to the original system.

$$\Lambda_1 = \frac{k_{\text{eff}}}{k} = 1 + \gamma_k \cot^2 \phi. \quad (64)$$

Next, the stiffness amplification factor will be derived for other inertial amplifier designs proposed here.

### 3.2. The Compound Stiffened Inertial Amplifier

The proposed design of a compound stiffened inertial amplifier with two cells is shown in Fig. 10.

Two secondary mechanisms are inserted within a primary mechanism as before. Each mass and stiffness within the cells are  $m_a/2$  and  $k_a/2$  so that the total mass and stiffness are the same as in the other proposed designs.



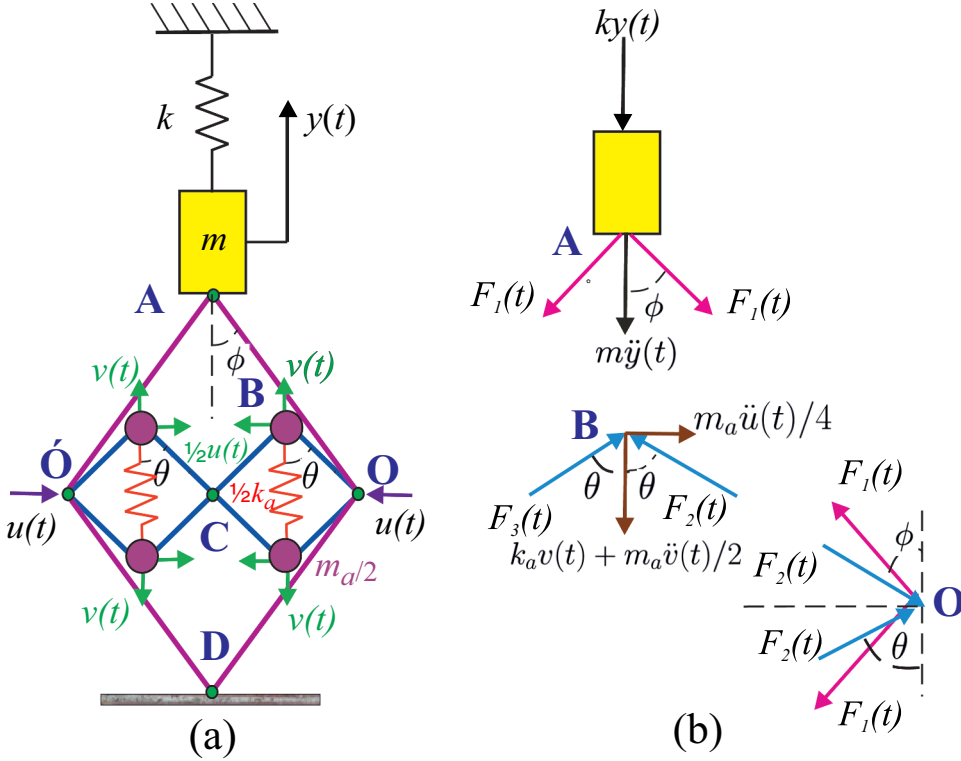


**Figure 10.** The compound stiffened inertial amplifier and its corresponding free-body diagram. (a) a compound stiffened inertial amplifier with two cells. The stiffness of the spring elements attached to mass within the cells is  $k_a/2$  so the total stiffness is  $k_a$  as in other inertial amplifiers. (b) The free-body diagram for the compound stiffened inertial amplifier.

The equation of motion can be obtained following the similar procedure outlined in [section 3](#) for the case of a pure inertial amplifier. The main difference arises from the equilibrium of forces in the vertical direction at point B. Considering that the spring  $k_a/2$  is stretched by  $2v(t)$ , the inertial forces are obtained as

$$\begin{aligned} F_2(t) \cos \theta + F_3(t) \cos \theta &= \frac{m_a}{2} \ddot{v}(t) + \frac{k_a}{2} 2v(t) \\ \text{or } F_2(t) + F_3(t) &= \frac{m_a \ddot{v}(t)/2 + k_a v(t)}{\cos \theta}. \end{aligned} \quad (65)$$

Adding this with Eq. (16) and eliminating  $F_3(t)$ , the expression of  $F_2(t)$  can be obtained as

$$2F_2(t) = \frac{m_a \ddot{v}(t)/2 + k_a v(t)}{\cos \theta} + \frac{m_a \ddot{u}(t)}{4 \sin \theta}. \quad (66)$$

Recalling from Eq. (12) that  $u(t) = y(t) \cot \phi/2$  and Eq. (14) that  $v(t) = \frac{y(t)}{4} \cot \phi \tan \theta$ , the total inertial forces are obtained as

$$2F_2(t) = \frac{m_a}{8} \cot \phi \left( \frac{\tan \theta}{\cos \theta} + \frac{1}{\sin \theta} \right) \ddot{y}(t) + \frac{k_a}{\cos \theta} \frac{y(t)}{4} \cot \phi \tan \theta. \quad (67)$$

Using Eq. (20), the inertial forces are obtained as

$$2F_1(t) \cos \phi = 2F_2(t) \sin \theta \cot \phi = \frac{m_a}{8} \cot^2 \phi (1 + \tan^2 \theta) \ddot{y}(t) + k_a y(t) \cot^2 \phi \frac{\tan^2 \theta}{4}. \quad (68)$$

Substituting this in the equilibrium of the mass at point A, from Eq. (21), the equation of motion has been obtained as

$$\underbrace{\left(m + \frac{m_a}{8} \cot^2 \phi (1 + \tan^2 \theta)\right)}_{m_{\text{eff}}} \ddot{y}(t) + \underbrace{\left(k + k_a \cot^2 \phi \frac{\tan^2 \theta}{4}\right)}_{k_{\text{eff}}} y(t) = 0. \quad (69)$$

The effective stiffness of the amplified system in Fig. 10 is  $(k + k_a \cot^2 \phi \frac{\tan^2 \theta}{4})$ . The above equation can be rewritten as

$$m(1 + \gamma_m (\cot^2 \phi (1 + \tan^2 \theta))/8) \ddot{y}(t) + k \left(1 + \gamma_k \cot^2 \phi \frac{\tan^2 \theta}{4}\right) y(t) = 0. \quad (70)$$

The non-dimensional stiffness amplification factor has been derived and defined as the ratio of the effective stiffness of the inertially amplified system to the original system.

$$\Lambda_2 = \frac{k_{\text{eff}}}{k} = 1 + \gamma_k \cot^2 \phi \frac{\tan^2 \theta}{4}. \quad (71)$$

If the compound inertial amplifier were to outperform the conventional amplifier in stiffness amplification, the required condition is

$$\Lambda_2 > \Lambda_1 \text{ or } 1 + \gamma_k \cot^2 \phi \frac{\tan^2 \theta}{4} > 1 + \gamma_k \cot^2 \phi \text{ or } \tan \theta > 2 \Rightarrow \theta > 64^\circ. \quad (72)$$

This requirement is in addition to  $\phi < 45^\circ$  required for the stiffness amplification from the conventional amplifier.

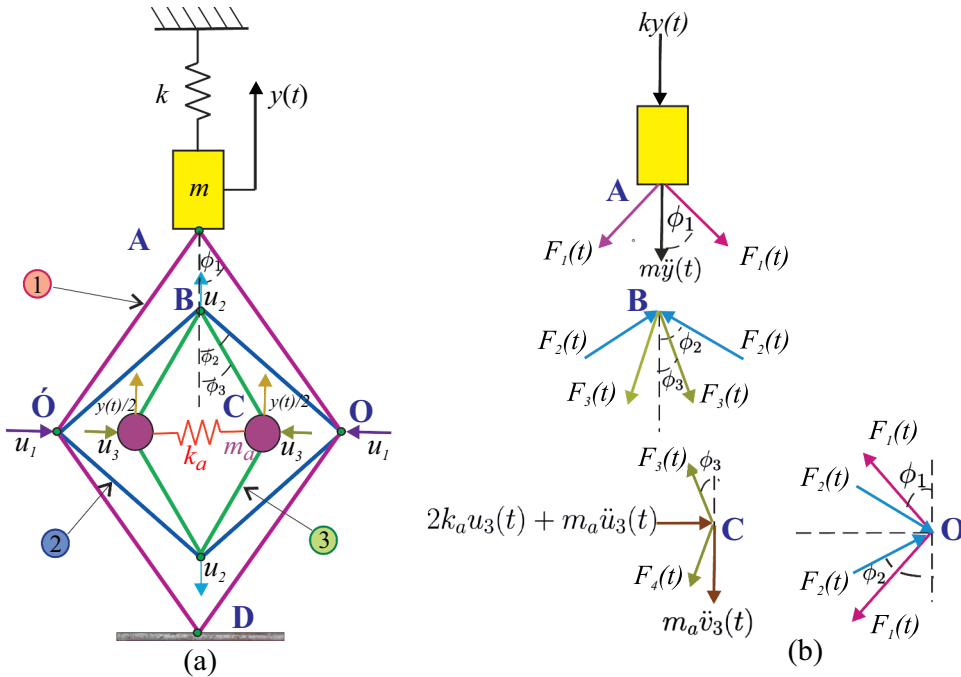


**Figure 11.** The nested stiffened inertial amplifier and its corresponding free-body diagram. (a) The stiffness of the spring element attached to mass within the inner cell is  $k_a$ . The amplifier angles for the mechanisms are  $\phi_1$ ,  $\phi_2$ , and  $\phi_3$  as shown. (b) The free-body diagram for the nested inertial amplifier.

### 3.3. The Nested Stiffened Inertial Amplifier

The proposed design of a nested stiffened inertial amplifier with three mechanisms is shown in Fig. 11.

The amplifier is obtained by introducing two connected four-bar rhombus mechanisms inside the primary mechanism. The spring with stiffness  $k_a$  is attached to the mass within the inner mechanism.

The equation of motion can be obtained following the similar procedure outlined in section 3 for the case of a pure inertial amplifier. The main difference arises from the equilibrium of forces in the horizontal direction at point C. Considering that the spring  $k_a$  is stretched by  $2u_3(t)$  and From the equilibrium of forces in the horizontal direction at point C, the inertial forces are derived as

$$F_3(t) \sin \phi_3 + F_4(t) \sin \phi_3 = m_a \ddot{u}_3(t) + 2k_a u_3(t) \quad (73)$$

$$\text{or } F_3(t) + F_4(t) = \frac{m_a \ddot{u}_3(t) + 2k_a u_3(t)}{\sin \phi_3}. \quad (74)$$

Adding Eqs. (34) and (73), the total inertial forces are derived as

$$2F_3(t) = \frac{m_a \ddot{v}_3(t)}{\cos \phi_3} + \frac{m_a \ddot{u}_3(t) + 2k_a u_3(t)}{\sin \phi_3}. \quad (75)$$

Following the analytical approach in Section 3 and after some simplifications, the equation of motion of an SDOF oscillator with the nested stiffened inertial amplifier is obtained as

$$\underbrace{\left( m + \frac{m_a}{2} (1 + \cot^2 \phi_3) \cot^2 \phi_1 \tan^2 \phi_2 \right)}_{m_{\text{eff}}} \ddot{y}(t) + \underbrace{\left( k + k_a \cot^2 \phi_1 (\tan^2 \phi_2 \cot^2 \phi_3) \right)}_{k_{\text{eff}}} y(t) = 0. \quad (76)$$

The effective stiffness of the amplified system in Fig. 10 is  $(k + k_a \cot^2 \phi_1 (\tan^2 \phi_2 \cot^2 \phi_3))$ . The above equation can be rewritten as

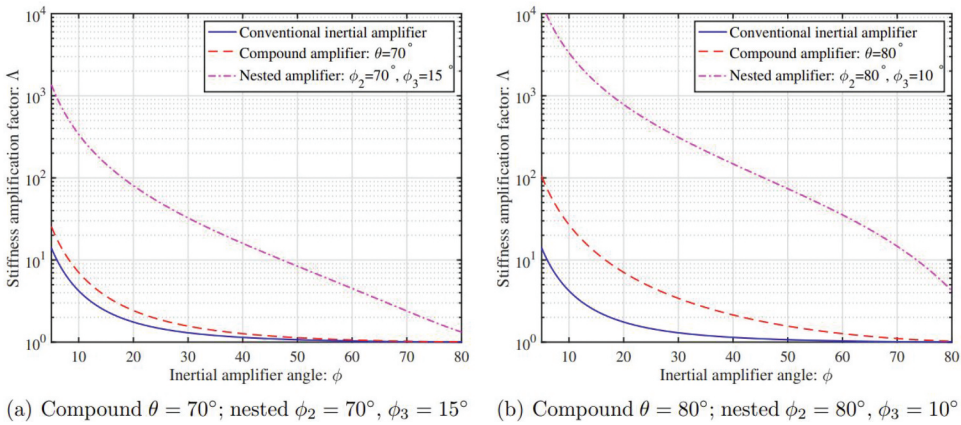


**Figure 12.** (a) Compound  $\theta = 70^\circ$ ; nested  $\phi_2 = 70^\circ$ ,  $\phi_3 = 15^\circ$  and (b) compound  $\theta = 80^\circ$ ; nested  $\phi_2 = 80^\circ$ ,  $\phi_3 = 10^\circ$ . Stiffness amplification as a function of the primary amplifier angle  $\phi$  for the conventional, compound, and nested amplifier SDOF system for various secondary amplifier angles  $\theta$ ,  $\phi_2$  and  $\phi_3$ . The value of the stiffness factor  $\gamma_k = 0.1$ . The compound and nested amplifiers show significantly more stiffness amplification compared to the conventional amplifier.

$$m(1 + \gamma_m(1 + \cot^2 \phi_3) \cot^2 \phi_1 \tan^2 \phi_2/2) \ddot{y}(t) + k(1 + \gamma_k \cot^2 \phi_1 (\tan^2 \phi_2 \cot^2 \phi_3)) y(t) = 0. \quad (77)$$

The non-dimensional stiffness amplification factor has been derived and defined as the ratio of the effective stiffness of the inertially amplified system to the original system.

$$\Lambda_3 = \frac{k_{\text{eff}}}{k} = 1 + \gamma_k \cot^2 \phi_1 (\tan^2 \phi_2 \cot^2 \phi_3). \quad (78)$$

In Fig. 12, the stiffness amplification from all the inertial amplifiers is compared.

The stiffness amplification factors  $\Lambda_i$ ,  $i = 1, 2, 3$  are plotted as a function of the primary amplifier angle  $\phi$ . The values of different secondary amplifier angles, such as  $\theta$ ,  $\phi_2$ , and  $\phi_3$  are shown in the plots. The compound and nested amplifiers show significantly more stiffness amplification compared to the conventional amplifier. In particular, the nested amplifier outperforms the other two amplifiers by orders of magnitude. This is analytically investigated below.

If the nested inertial amplifier outperforms the conventional amplifier in the stiffness amplification, the required condition is

$$\Lambda_3 > \Lambda_1 \quad \text{or} \quad 1 + \gamma_k \cot^2 \phi_1 (\tan^2 \phi_2 \cot^2 \phi_3) > 1 + \gamma_k \cot^2 \phi_1 \quad \text{or} \quad \tan \phi_2 \cot \phi_3 > 1. \quad (79)$$

Therefore, the nested amplifier will outperform the ordinary amplifier provided the same conditions for the case of inertial amplification given by Eq. (44) are satisfied. In Fig. 12, it can be observed that the nested amplifier, in general, results in more stiffness amplification compared to the compound amplifier. This happens when

$$\Lambda_3 > \Lambda_2 \quad \text{or} \quad \cot^2 \phi_1 (\tan^2 \phi_2 \cot^2 \phi_3) > \cot^2 \phi_1 \frac{\tan^2 \theta}{4} \quad \text{or} \quad \tan \phi_2 \cot \phi_3 > \frac{1}{2} \tan \theta. \quad (80)$$

If this condition is satisfied, it will automatically satisfy the condition in Eq. (79). This can be observed in Fig. 12 also. Therefore, it can be concluded that it is possible to obtain physically realistic parameters

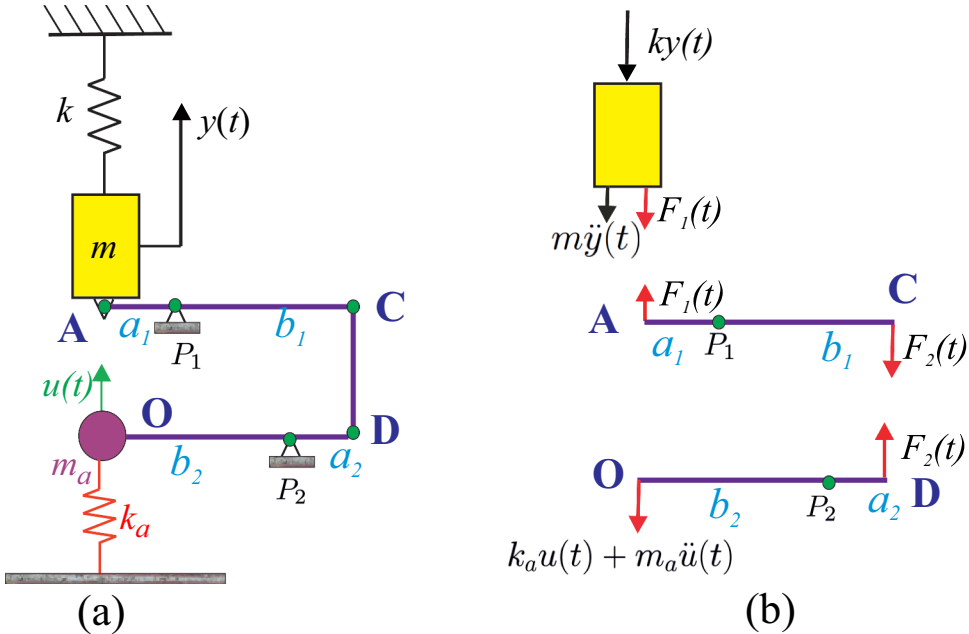


**Figure 13.** (a) The stiffened levered inertial amplifier is made of three connected rigid levers. The spring with stiffness  $k_a$  is connected with the lever arm at point O. The lever arms can freely pivot about the points  $P_1$  and  $P_2$ . (b) The free-body diagram for the levered inertial amplifier.

such that the stiffness amplification of the three amplifier configurations satisfies the following inequality

$$\Lambda_3 \geq \Lambda_2 \geq \Lambda_1. \quad (81)$$

Next, the stiffness amplification of the levered inertial amplifier has been derived and introduced.

### 3.4. The Levered Inertial Amplifier

The proposed design of a stiffened levered inertial amplifier is shown in Fig. 13.

The spring with stiffness  $k_a$  is connected with the second lever arm at point O. The rods AC, CD, and DO are assumed to be rigid. In addition, the rod AC pivots freely about  $P_1$ , and the rod DO pivots freely about  $P_2$ . The rod CD simply connects rods AC and DO and transfers the motion.

The equation of motion can be obtained following the similar procedure outlined in section 3 for the case of a pure inertial amplifier. The main difference arises from the equilibrium of forces in the vertical direction at point O. Considering that the spring  $k_a$  is stretched by  $u(t)$ , taking a moment about  $P_2$  for the rigid link OD, the inertial force has been derived as

$$F_2(t)a_1 = (m_a\ddot{u}(t) + k_a u(t))b_2. \quad (82)$$

Using the expression of  $u(t)$  from Eq. (48) and substituting in the equilibrium Eq. (49), the equation of motion of an SDOF oscillator with the levered stiffened inertial amplifier is obtained as

$$\underbrace{\left(m + m_a \left(\frac{b_1 b_2}{a_1 a_2}\right)^2\right)}_{m_{\text{eff}}} \ddot{y}(t) + \underbrace{\left(k + k_a \left(\frac{b_1 b_2}{a_1 a_2}\right)^2\right)}_{k_{\text{eff}}} y(t) = 0. \quad (83)$$

The effective stiffness of the amplified system in Fig. 10 is  $\left(k + k_a \left(\frac{b_1 b_2}{a_1 a_2}\right)^2\right)$ . The non-dimensional stiffness amplification factor has been derived and defined as the ratio of the effective stiffness of the inertially amplified system to the original system

$$\Lambda_4 = \frac{k_{\text{eff}}}{k} = 1 + \gamma_k \left(\frac{b_1 b_2}{a_1 a_2}\right)^2. \quad (84)$$

The stiffness amplification factor is similar to the inertial amplification factor obtained before in Eq. (54).

If the levered inertial amplifier was to outperform the conventional amplifier in the stiffness amplification, the required condition is

$$\Lambda_4 > \Lambda_1 \quad \text{or} \quad 1 + \gamma_k \left(\frac{b_1 b_2}{a_1 a_2}\right)^2 > 1 + \gamma_k \cot^2 \phi \quad \text{or} \quad \frac{b_1 b_2}{a_1 a_2} > \cot \phi. \quad (85)$$

This requirement, along with the requirement of inertial amplification derived in Eq. (56), will ensure that the stiffened levered inertial amplifier outperforms the conventional inertial amplifier in both inertial and stiffness amplifications. To understand both the requirements, in Fig. 14, the minimum lever arm ratio necessary for the levered inertial amplifier to outperform the conventional stiffened inertial amplifier in both fronts is shown as a function of the amplifier angle  $\phi$ .

The shaded area shows the region of lever arm ratio for which the levered amplifier has a higher inertial amplification but a lower stiffness amplification in comparison to the conventional amplifier.

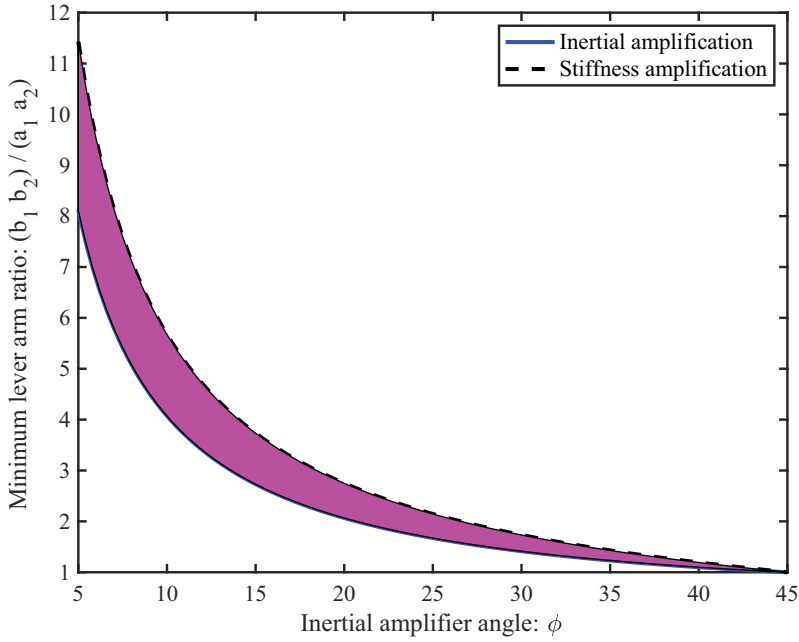


**Figure 14.** The minimum lever arm ratio necessary for the stiffened levered inertial amplifier to outperform the conventional stiffened inertial amplifier is shown as a function of the amplifier angle  $\phi$ .

#### 4. Natural Frequency Tuning and Iso-Spectral Systems

It was observed that the stiffened inertial amplifiers change the effective mass and stiffness of the underlying SDOF oscillator. This naturally implies that the resonance frequency of the oscillator will be different and will change with the parameters of the inertial amplifiers. This gives an outstanding opportunity to tune the effective resonance frequency. This can be exploited in a wide range of beneficial ways in practical applications. For example, stiffened inertial amplifiers can be incorporated to shift the natural frequency of a system from a predominant excitation resonance frequency for vibration mitigation.

In this section, the fundamental analytical methods for controlling the effective natural frequency have been derived. As there are many parameters, this can be achieved in a number of ways. The mass of the amplifier  $m_a$  is often selected first (say  $\gamma_m < 0.2$ ) from wider considerations (such as weight constraints). Therefore, the aim is to obtain the stiffness of the inertial amplifiers for a desired change in the effective resonance frequency.

##### 4.1. Natural Frequency Tuning

The resonance frequency of the baseline oscillator is given by

$$\omega_0 = \sqrt{\frac{k}{m}}. \quad (86)$$

The aim is to shift the resonance frequency of the inertially amplified oscillator in a desired and controlled manner. The equation of motion of the inertially amplified oscillator can be expressed in a general form as

$$m\Gamma_i \ddot{y}(t) + k\Lambda_i y(t) = 0, \quad i = 1, 2, 3, 4. \quad (87)$$

In the above, the indices 1, 2, 3, and 4 denote the conventional, compound, nested, and levered inertial amplifier configurations. The natural frequency of the inertially amplified oscillator  $\omega_a$  is given by

$$\omega_a = \omega_0 \sqrt{\frac{\Lambda_i}{\Gamma_i}}. \quad (88)$$

In the above  $\Lambda_i$  and  $\Gamma_i$  are the stiffness and inertial amplification factors for the four configurations derived in the previous two sections. The frequency tuning parameter  $c$  is introduced and defined as the ratio between the natural frequency of the inertially amplified oscillator and the baseline oscillator

$$\frac{\omega_a}{\omega_0} = \sqrt{\frac{\Lambda_i}{\Gamma_i}} = c. \quad (89)$$

The value of  $c$  can be selected for the desired frequency tuning. As the proposed inertial amplifier designs can generate a wide range of effective mass and stiffness variations, it is expected that a feasible solution can be found for a greater range of  $c$ . For notation convenience, the stiffness and inertial amplification factors are rewritten as

$$\Lambda_i = 1 + \gamma_k f_i \quad \text{and} \quad \Gamma_i = 1 + \gamma_m g_i. \quad (90)$$

Here  $f_i$  and  $g_i$  are functions of only the geometric parameters of the inertial amplifiers. They can be identified from the derivations in the previous sections as

$$\begin{aligned} f_1 &= \cot^2 \phi, f_2 = \cot^2 \phi \frac{\tan^2 \theta}{4}, \\ f_3 &= \cot^2 \phi_1 (\tan^2 \phi_2 \cot^2 \phi_3), \quad \text{and} \quad f_4 = \left( \frac{b_1 b_2}{a_1 a_2} \right)^2. \end{aligned} \quad (91)$$

$$\begin{aligned} g_1 &= (1 + \cot^2 \phi)/2, g_2 = (\cot^2 \phi (1 + \tan^2 \theta))/8, \\ g_3 &= (1 + \cot^2 \phi_3) \cot^2 \phi_1 \tan^2 \phi_2 / 2, \quad \text{and} \quad g_4 = \left( \frac{b_1 b_2}{a_1 a_2} \right)^2. \end{aligned} \quad (92)$$

Substituting Eqs. (90) in (89) and solving, the desired value of the stiffness factor  $\gamma_k$  is derived for a given  $\gamma_m$  as

$$\frac{1 + \gamma_k f_i}{1 + \gamma_m g_i} = c^2 \quad \text{or} \quad \gamma_k = \frac{\gamma_m f_i + (1 - c^2)}{c^2 g_i}, \quad i = 1, 2, 3, 4. \quad (93)$$

Using this solution, the exact analytical expression for the stiffness factor can be explicitly obtained for the four inertial amplifiers as

$$\gamma_k = 1/2 \frac{(1 + (\cot(\phi))^2) \gamma_m}{c^2 (\cot(\phi))^2} + \frac{-c^2 + 1}{c^2 (\cot(\phi))^2} \quad (\text{conventional}). \quad (94)$$

$$\gamma_k = 1/2 \frac{(1 + (\tan(\theta))^2) \gamma_m}{c^2 (\tan(\theta))^2} + 4 \frac{-c^2 + 1}{c^2 (\cot(\phi))^2 (\tan(\theta))^2} \quad (\text{compound}). \quad (95)$$

$$\gamma_k = 1/2 \frac{(1 + (\cot(\phi_3))^2) \gamma_m}{c^2 (\cot(\phi_3))^2} + \frac{-c^2 + 1}{c^2 (\cot(\phi_3))^2 (\cot(\phi_1))^2 (\tan(\phi_2))^2} \quad (\text{nested}). \quad (96)$$

$$\gamma_k = \frac{\gamma_m}{c^2} + \frac{-c^2 + 1}{c^2 \alpha^2}, \alpha = \frac{b_1 b_2}{a_1 a_2} \quad (\text{levered}). \quad (97)$$

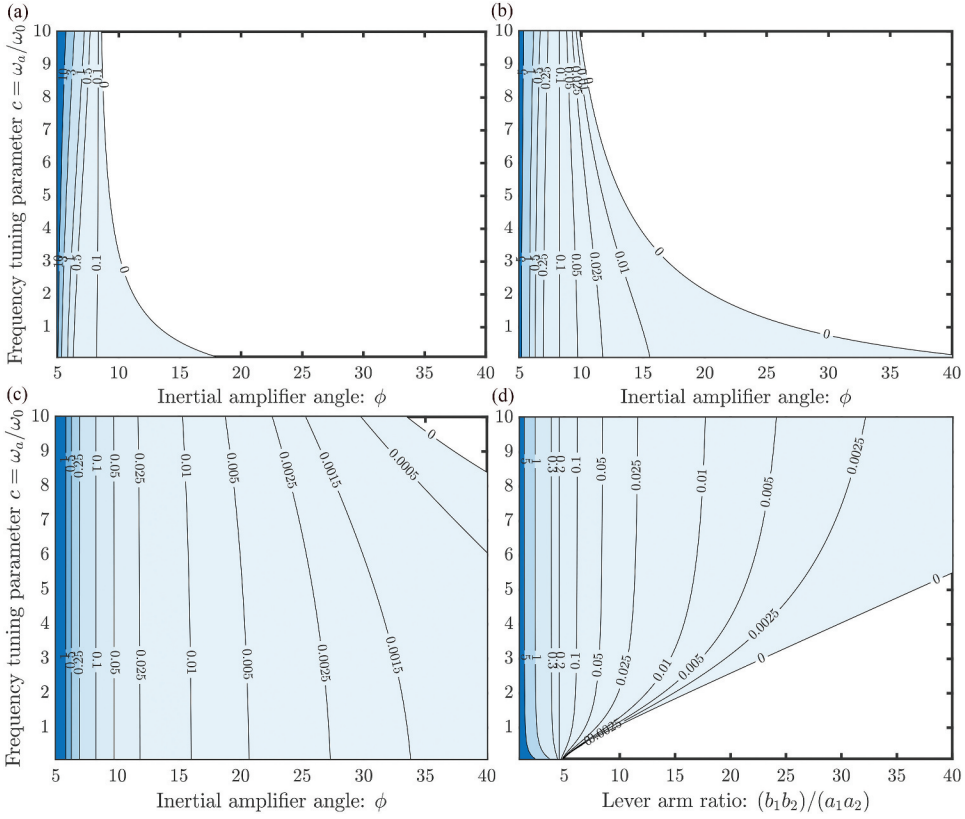


**Figure 15.** The contours of the stiffness factor  $\gamma_k$  with  $\gamma_m = 0.2$  for the (a) conventional, (b) compound:  $\theta = 80^\circ$ , (c) nested:  $\phi_2 = 80^\circ, \phi_3 = 10^\circ$ , and (d) levered stiffened amplifiers. The results are shown for frequency tuning parameter  $c = \omega_a/\omega_0$  in the y-axis and the primary amplifier angle in the x-axis (and lever arm ratio for the levered amplifier). The unshaded regions indicate that no feasible value of  $\gamma_k$  is possible.

The first part of the above expressions is a function of  $\gamma_m$ , while the second part depends only on the tuning factor  $c$  and geometric parameters of the inertial amplifier. In Fig. 15, contours of the stiffness factor,  $\gamma_k$  obtained from the above equations for the four inertial amplifier configurations are shown.

A fixed value of  $\gamma_m = 0.2$  is used in the calculations. The unshaded regions in the plots indicate no feasible value of  $\gamma_k$  is possible. The frequency tuning parameter  $c = \omega_a/\omega_0$  is varied from 0.1 to 10. The results show that for the rhombus-based inertial amplifier designs, significant control of the natural frequency is possible for smaller primary amplifier angles. For the levered amplifier, a very small value of the stiffness factor  $\gamma_k$  is necessary for frequency tuning if the lever arm ratio is larger. The tuning capability demonstrated here can be exploited in practical applications for vibration mitigation.

#### 4.2. Iso-Spectral Systems

In some applications, it may not be desirable that the natural frequency would change due to the employment of an inertial amplifier. This may result in an unwanted resonance that was originally designed to be avoided for a dynamic system. Therefore, it is of practical interest to have a realistic stiffened inertial amplifier that will not alter the undamped natural frequency of the baseline system. From Eq. (89), this requirement translates to  $c = 1$ . This type of dynamic system is called an iso-spectral system. This is a special case of the general results derived in the previous section. Therefore, substituting  $c = 1$  in Eqs. (94)–(97), the necessary stiffness factor for iso-spectral systems are derived as



$$\frac{\gamma_k}{\gamma_m} = \frac{1}{2} \sec^2 \phi \quad (\text{conventional}) \quad (98)$$

$$\frac{\gamma_k}{\gamma_m} = \frac{1}{2} \operatorname{cosec}^2 \theta \quad (\text{compound}) \quad (99)$$

$$\frac{\gamma_k}{\gamma_m} = \frac{1}{2} \sec^2 \phi_3 \quad (\text{nested}) \quad (100)$$

$$\frac{\gamma_k}{\gamma_m} = 1 \quad (\text{levered}) \quad (101)$$

It is interesting to note that the stiffness factor is independent of the primary amplifier angle for the compound and nested amplifiers. Therefore, if an iso-spectral system is to be designed, any primary amplifier angle can be chosen for these configurations. For the levered amplifier, the stiffness factor needs to be the same as the mass factor for an iso-spectral system. These simple design guidelines can help to obtain a stiffened inertially amplified oscillatory iso-spectral SDOF system.

### 4.3. Dynamic Response Analysis

Previous subsections provide a theoretical approach towards quantifying dynamic characteristics and parameter selection of the inertial amplifiers. In this section, it has been explicitly demonstrated the impact of the inertial amplifiers on the dynamic response of an SDOF oscillator. Frequency domain response is considered. It is necessary to consider damping to have a finite response at the resonance. The equation of motion of the inertially amplified damped oscillator can be expressed in a general form by the addition of a damping term to Eq. (87) as

$$m\Gamma_i \ddot{y}(t) + d\dot{y} + k\Lambda_i y(t) = f(t), \quad i = 0, 1, 2, 3, 4. \quad (102)$$

Here  $d$  is the damping coefficient, and  $f(t)$  is the forcing function. In the above equation,  $i = 0$  corresponds to the baseline oscillator, that is, the oscillator without any attached inertial amplifier. For  $i = 0$ , it is obvious that  $\Gamma_0 = \Lambda_0 = 1$  in Eq. (102). For  $i = 1, \dots, 4$ ,  $\Gamma_i$  and  $\Lambda_i$  are explicitly defined through Eqs. (90)–(92).

Considering a harmonic forcing and harmonic response (assuming the steady-state response), one has

$$f(t) = F(\omega) \exp\{j\omega t\} \quad \text{and} \quad y(t) = Y(\omega) \exp\{j\omega t\}. \quad (103)$$

Here  $j = \sqrt{-1}$ ,  $\omega$  is the frequency,  $F(\omega)$  is the frequency domain forcing and  $Y(\omega)$  is the frequency domain response. Substituting these in the equation of motion Eq. (102) one has

$$(-\omega^2 m\Gamma_i + jd + k\Lambda_i) Y(\omega) = F. \quad (104)$$

As the forcing is considered to be purely harmonic,  $F(\omega) \equiv F$  is used in the above equation. Dividing by  $m$  one has

$$(-\omega^2 \Gamma_i + 2j\omega\zeta\omega_0 + \omega_0^2 \Lambda_i) Y(\omega) = F/m. \quad (105)$$

Where the damping factor  $\zeta_0$  is defined as

$$\frac{d}{m} = 2\zeta\omega_0. \quad (106)$$

and  $\omega_0$  is defined in Eq. (86). Dividing Eq. (105) by  $\omega_0^2$  and rearranging, the generalized response of inertially amplified SDOF oscillator can be obtained as

$$Y(\omega) = \frac{F/k}{-\Omega^2 \Gamma_i + 2j\Omega\zeta + \Lambda_i}. \quad (107)$$

where the normalized frequency

$$\Omega = \frac{\omega}{\omega_0}. \quad (108)$$

Note that the static deflection of the oscillator is given by

$$y_{st} = \frac{F}{k}. \quad (109)$$

The normalized dynamic response amplitude is, therefore, given by

$$\frac{|Y(\omega)|}{y_{st}} = \frac{1}{\sqrt{(\Lambda_i - \Omega^2 \Gamma_i)^2 + (2\Omega\zeta)^2}}. \quad (110)$$

For numerical calculations, the ratio between the stiffness and mass is formulated through Eq. (89). In Fig. 16, three values of  $c$  and two values and two values of  $\zeta$  have been employed.

For the conventional, compound, and nested inertial amplifiers, a fixed value of  $\phi = 15^\circ$  is selected. Additionally, for the compound inertial amplifier,  $\theta = 80^\circ$  and the nested inertial amplifier,  $\phi_2 = 70^\circ$  and  $\phi_3 = 15^\circ$  have been used. For the levered inertial amplifier, a lever arm ratio of  $\frac{b_1}{a_1} \frac{b_2}{a_2} = 5$  is selected. The mass ratio  $\gamma_m = 0.2$  is employed and the stiffness ratio  $\gamma_k$  is obtained from Eqs. (94)–(97) for the chosen values of the other parameters for the four inertial amplifiers as described. It is clear from

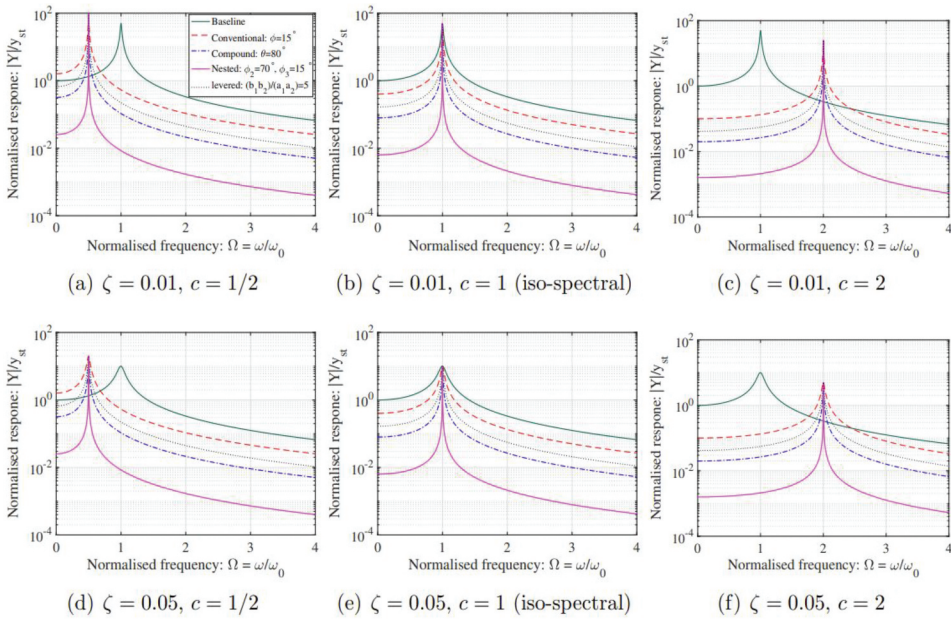


**Figure 16.** (a)  $\zeta = 0.01$ ,  $c = 1/2$ , (b)  $\zeta = 0.01$ ,  $c = 1$  (iso-spectral), (c)  $\zeta = 0.01$ ,  $c = 2$ , (d)  $\zeta = 0.05$ ,  $c = 1/2$ , (e)  $\zeta = 0.05$ ,  $c = 1$  (iso-spectral), and (f)  $\zeta = 0.05$ ,  $c = 2$ . Dynamic response of inertially amplified single-degree-of-freedom (SDOF) damped oscillators in the frequency domain. Three values of the frequency tuning parameter  $c$  are considered. Two values of the damping coefficient  $\zeta$  are considered. The mass ratio  $\gamma_m = 0.2$  is selected, and the stiffness ratio  $\gamma_k$  is obtained from Eqs. (94)–Eq. (97) for the given values of the other parameters for the four inertial amplifiers.

Fig. 16 that in general, the inertially amplified oscillators have a significantly lower dynamic response. For the  $c < 1$  design, the maximum response is slightly more than the maximum response of the baseline oscillators. On the other hand, an opposite observation is made when  $c > 1$ . The numerical results obtained in Fig. 16, demonstrate a huge potential for manipulating the dynamic response of a conventional SDOF oscillator with attached inertial amplifiers.

## 5. Vibration Control Using Stiffened Inertial Amplifiers

The stiffened inertial amplifiers are induced inside the core material of the conventional nonlinear friction base isolators to enhance their vibration reduction capacity and overcome their limitations. Four single-story buildings with the same governing system parameters, i.e. mass, stiffness, and damping, are isolated by stiffened inertial amplifier base isolator, compound stiffened inertial amplifier base isolator, nested stiffened inertial amplifier base isolator, and levered inertial amplifier base isolator. The single-story buildings are conceptualized as single-degree-of-freedom systems. The isolated single-degree-of-freedom systems are subjected to base excitation. The structural diagrams of each isolated single-degree-of-freedom systems have been shown in Fig. 17a–d.

Newton's second law has been employed to derive the governing equations of motion of each isolated single-degree-of-freedom system. The governing equation of motion of the isolated single-degree-of-freedom system has been derived as

$$m_s \ddot{v}_s + m_s \ddot{v}_b + c_s \dot{v}_s + k_s v_s = -m_s \ddot{v}_g. \quad (111)$$

The governing equation of motion of the novel isolator has been derived as

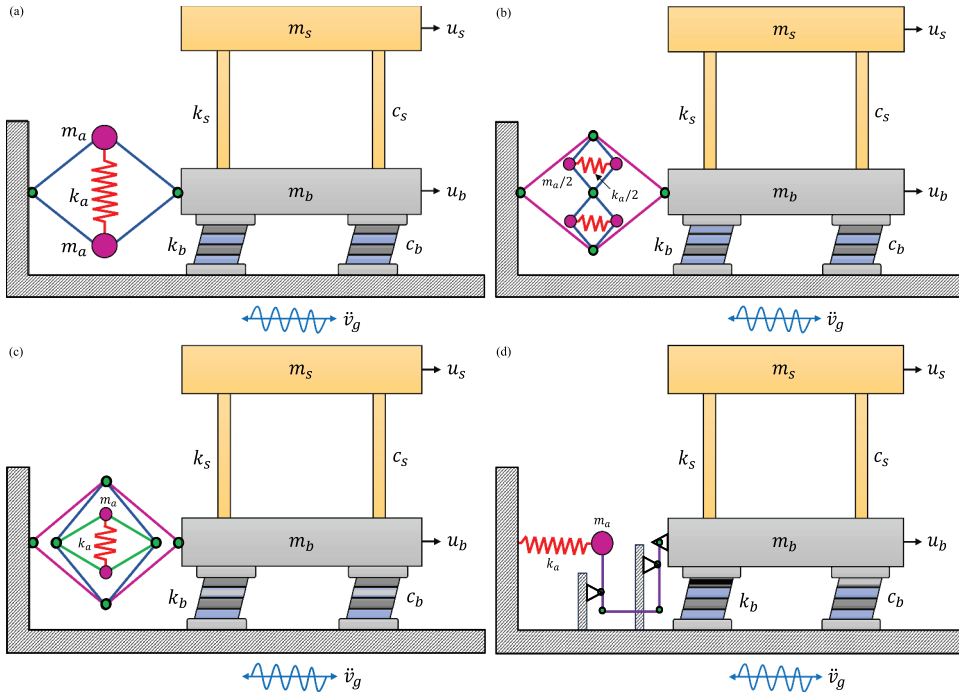


**Figure 17.** Four single-degree-of-freedom systems are isolated by a stiffened inertial amplifier base isolator, compound stiffened inertial amplifier base isolator, nested stiffened inertial amplifier base isolator, and levered inertial amplifier base isolator subjected to base excitation. The governing system parameters of the main structures, i.e. single-degree-of-freedom systems, are considered the same to conduct a fair comparison between each novel isolator and conventional base isolator in terms of vibration reduction capacity.

**Table 1.** The exact closed-form expressions for effective mass and stiffness of novel isolators.

Isolator	Effective mass ( $m_e$ )	Effective stiffness ( $k_e$ )
SIABI	$(m_b + \frac{m_a}{2}(1 + \cot^2 \phi))$	$(k_b + k_a \cot^2 \phi)$
CSIABI	$(m_b + \frac{m_a}{8} \cot^2 \phi (1 + \tan^2 \theta))$	$(k_b + k_a \cot^2 \phi \frac{\tan^2 \theta}{4})$
NSIABI	$(m_b + \frac{m_a}{2}(1 + \cot^2 \phi_3) \cot^2 \phi_1 \tan^2 \phi_2)$	$(k_b + k_a \cot^2 \phi_1 (\tan^2 \phi_2 \cot^2 \phi_3))$
LSIABI	$(m_b + m_a (\frac{b_1 b_2}{a_1 a_2})^2)$	$(k_b + k_a (\frac{b_1 b_2}{a_1 a_2})^2)$

SIABI: stiffened inertial amplifier base isolator (Eq. (61)).

CSIABI: compound stiffened inertial amplifier base isolator (Eq. (69)).

NSIABI: nested stiffened inertial amplifier base isolator (Eq. (76)).

LSIABI: levered stiffened inertial amplifier base isolator (Eq. (83)).

$$m_e \ddot{v}_b + c_e \dot{v}_b + k_e v_b - c_s \dot{v}_s - k_s v_s = -m_e \ddot{v}_g, \quad (112)$$

where  $v_s = u_s - u_b$  and  $v_b = u_b - v_g$  define the relative deflection of the single-degree-of-freedom systems and the isolators. The exact closed-form expressions for effective mass and stiffness for each isolator are listed in Table 1.

Table 1 is applied in Eq. (112) and the governing equation of motion for the stiffened inertial amplifier base isolator, compound stiffened inertial amplifier base isolator, nested stiffened inertial amplifier base isolator, and levered stiffened inertial amplifier base isolator have been derived. Table 1 is represented in non-dimensional form to perform the  $H_\infty$  optimization method and is listed in Table 2. Table 2 presents the exact closed-form expressions for the non-dimensional effective mass and stiffness of the novel isolator.

$\gamma_b = m_b/m_s$  defines the mass ratio of isolator to the single-degree-of-freedom system.  $\gamma_m = m_a/m_b$  defines the mass ratio of amplifier to the isolator.

$\gamma_m$  has also been represented as  $\gamma_m = \gamma_a/\gamma_b$ .  $\gamma_a = m_a/m_s$  defines the mass ratio of amplifier to the single-degree-of-freedom system.  $\gamma_k = k_a/k_b$  defines the stiffness ratio of amplifier stiffness to the isolator.

As the isolated single-degree-of-freedom systems are subjected to base excitation, the steady-state solutions are considered as  $v_s = V_s e^{i\omega t}$ ,  $v_b = V_b e^{i\omega t}$ , and  $\ddot{v}_g = V_g e^{i\omega t}$ . The steady-state solutions are substituted in Eq. (111) and Eq. (112) to derive the frequency response function for obtaining dynamic responses of the isolated single-degree-of-freedom systems in the frequency domain. In addition, the  $H_\infty$  optimization method has been applied to derive exact closed-form expressions for the optimal

**Table 2.** The non-dimensional form of effective mass and stiffness of novel isolators.

Isolator	Effective mass ratio	Effective stiffness
SIABI	$\gamma_b \left( 1 + \gamma_m \underbrace{(1 + \cot^2 \phi)/2}_{\mu} \right)$	$\gamma_b \omega_b^2 \left( 1 + \gamma_k \underbrace{\cot^2 \phi}_{\kappa} \right)$
CSIABI	$\gamma_b \left( 1 + \gamma_m \underbrace{(\cot^2 \phi (1 + \tan^2 \theta))/8}_{\mu} \right)$	$\gamma_b \omega_b^2 \left( 1 + \gamma_k \underbrace{\cot^2 \phi \frac{\tan^2 \theta}{4}}_{\kappa} \right)$
NSIABI	$\gamma_b \left( 1 + \gamma_m \underbrace{(1 + \cot^2 \phi_3) \cot^2 \phi_1 \tan^2 \phi_2/2}_{\mu} \right)$	$\gamma_b \omega_b^2 \left( 1 + \gamma_k \underbrace{\cot^2 \phi_1 (\tan^2 \phi_2 \cot^2 \phi_3)}_{\kappa} \right)$
LSIABI	$\gamma_b \left( 1 + \gamma_m \underbrace{\left( \frac{b_1 b_2}{a_1 a_2} \right)^2}_{\mu} \right)$	$\gamma_b \omega_b^2 \left( 1 + \gamma_k \underbrace{\left( \frac{b_1 b_2}{a_1 a_2} \right)^2}_{\kappa} \right)$

$\mu$  = Mass amplification factor of the isolators.  $\kappa$  = Stiffness amplification factor of the isolators.  $\gamma_e = m_e/m_s$ : Effective mass ratio  $\epsilon_e = k_e/m_s$ : Effective stiffness

design parameters of the novel base isolators. To apply this optimization method, the damping of the single-degree-of-freedom system has been considered zero, i.e.  $\xi_s = 0$ . Accordingly,  $\xi_s = 0$  has been substituted in Eq. (111) and Eq. (112) and the entire frequency response function is divided by the square of the natural frequency of the single-degree-of-freedom system, i.e.  $\omega_s^2$ , to make it non-dimensionalized. Accordingly, the frequency response function has been derived as

$$\begin{bmatrix} A_{11} & -1 \\ -\eta^2 & -\eta^2 + 1 \end{bmatrix} \begin{Bmatrix} V_b \\ V_s \end{Bmatrix} = - \begin{bmatrix} \gamma_b(\gamma_m \mu + 1) \\ 1 \end{bmatrix} \frac{V_g}{\omega_s^2}, \quad (113)$$

$$A_{11} = -\gamma_b(\mu\gamma_m + 1)\eta^2 + 2i\gamma_b(\mu\gamma_m + 1)\xi_b\eta_b\eta + \gamma_b\eta_b^2(\kappa\gamma_k + 1).$$

where  $\eta = \omega/\omega_s$  defines the frequency ratio of the excitation to the single-degree-of-freedom system. The dynamic response of the single-degree-of-freedom system has been derived as

$$X_s = \left(\frac{V_s}{V_g}\right)\omega_s^2 = \frac{\eta_b^2\kappa\gamma_b\gamma_k + \gamma_b\eta_b^2 + i(2\eta\eta_b\mu\xi_b\gamma_b\gamma_m + 2\gamma_b\xi_b\eta_b\eta)}{\Delta_e}. \quad (114)$$

The dynamic response of the isolator has been derived as

$$X_b = \left(\frac{V_b}{V_g}\right)\omega_s^2 = \frac{-\eta^2\mu\gamma_b\gamma_m - \gamma_b\eta^2 + \mu\gamma_b\gamma_m + \gamma_b + 1}{\Delta_e}. \quad (115)$$

The denominator of Eqs. (114) and (115) has been derived as

$$\Delta_e = \begin{pmatrix} -\eta^4\mu\gamma_b\gamma_m + \eta^2\eta_b^2\kappa\gamma_b\gamma_k - \eta^4\gamma_b + \eta^2\eta_b^2\gamma_b \\ +\eta^2\mu\gamma_b\gamma_m - \eta_b^2\kappa\gamma_b\gamma_k + \eta^2\gamma_b - \eta_b^2\gamma_b + \eta^2 \\ +i\xi_b(2\eta^3\gamma_m\mu\eta_b\gamma_b + 2\eta^3\eta_b\gamma_b - 2\eta\gamma_m\mu\eta_b\gamma_b - 2\eta\gamma_b\eta_b) \end{pmatrix}. \quad (116)$$

The resultant of Eq. (114) has been applied to derive constraints and expressed as

$$X_s = \sqrt{\frac{R_1^2 + \xi_b^2 R_2^2}{R_3^2 + \xi_b^2 R_4^2}}. \quad (117)$$

The closed-form expressions for  $R_1$  to  $R_4$  have been derived as

$$\begin{aligned} R_1 &= \gamma_b\eta_b^2\kappa\gamma_k + \gamma_b\eta_b^2, \\ R_2 &= 2\eta\eta_b\mu\gamma_b\gamma_m + 2\eta\eta_b\gamma_b, \\ R_3 &= \begin{aligned} &-\eta^4\mu\gamma_b\gamma_m + \eta^2\eta_b^2\kappa\gamma_b\gamma_k - \eta^4\gamma_b + \eta^2\eta_b^2\gamma_b \\ &+\eta^2\mu\gamma_b\gamma_m - \gamma_b\eta_b^2\kappa\gamma_k + \eta^2\gamma_b - \gamma_b\eta_b^2 + \eta^2 \end{aligned}, \\ R_4 &= 2\eta^3\eta_b\mu\gamma_b\gamma_m + 2\eta^3\eta_b\gamma_b - 2\eta\eta_b\mu\gamma_b\gamma_m - 2\eta\eta_b\gamma_b. \end{aligned} \quad (118)$$

Two constraints are derived as follows.

$$\left.\frac{R_1}{R_2}\right|_{\eta_j} = \left.\frac{R_3}{R_4}\right|_{\eta_j} \quad \text{and} \quad \left.\frac{R_3}{R_4}\right|_{\eta_1} = \left.\frac{R_3}{R_4}\right|_{\eta_2}. \quad (119)$$

Eq. (118) has been substituted in the first constraint of Eq. (119). As a result, an equation has been derived which contains the optimal natural frequency of the isolators and expressed as

$$(\mu\gamma_b\gamma_m + \gamma_b)\eta^4 + (-2\gamma_b\eta_b^2\kappa\gamma_k - 2\gamma_b\eta_b^2 - \mu\gamma_b\gamma_m - \gamma_b - 1)\eta^2 + 2\gamma_b\eta_b^2\kappa\gamma_k + 2\gamma_b\eta_b^2 = 0. \quad (120)$$

The summation of two roots from Eq. (120) has been derived as

$$\eta_1^2 + \eta_2^2 = \frac{1 + (\mu\gamma_m + 1 + (2\kappa\gamma_k + 2)\eta_b^2)\gamma_b}{\gamma_b(\mu\gamma_m + 1)}. \quad (121)$$

Eq. (118) has been substituted in the second constraint of Eq. (119) and as a result, the summation of two roots is derived as

$$\eta_1^2 + \eta_2^2 = 2. \quad (122)$$

Eq. (121) and Eq. (122) are equated and the exact closed-form expression for the optimal natural frequency of the isolator has been derived as

$$(\eta_b)_{opt} = \frac{\sqrt{2} \sqrt{\gamma_b(\kappa\gamma_k + 1)(\mu\gamma_b\gamma_m + \gamma_b - 1)}}{2\gamma_b(\kappa\gamma_k + 1)}. \quad (123)$$

The individual expression for each root, i.e.  $\eta_1^2$  and  $\eta_2^2$ , has been derived as

$$\eta_{1,2}^2 = \frac{1 + \mu\gamma_m \pm \sqrt{-2\eta_b^2\kappa\mu\gamma_k\gamma_m - 2\eta_b^2\kappa\gamma_k - 2\eta_b^2\mu\gamma_m + \mu^2\gamma_m^2 - 2\eta_b^2 + 2\mu\gamma_m + 1}}{\mu\gamma_m + 1}. \quad (124)$$

The closed-form expression for the optimal damping ratio of the isolator has been derived by formulating a mathematical expression and expressed as

$$\left. \frac{\partial |X_s|^2}{\partial \eta^2} \right|_{\eta_{1,2}} = 0 \quad \text{and} \quad (\xi_b)_{opt} = \sqrt{\frac{\xi_{b1}^2 + \xi_{b2}^2}{2}}. \quad (125)$$

Eq. (117) has been substituted in the first expression of Eq. (125) and the closed-form expression for optimal damping ratio of the isolator has been derived as

$$\begin{aligned} E_1\xi_b^4 + E_2\xi_b^2 + E_3 &= 0, \\ (\xi_{b1,b2})_{\eta_{1,2}}^2 &= \frac{-E_2 \pm \sqrt{E_2^2 - 4E_1E_3}}{2E_1}. \end{aligned} \quad (126)$$

The closed-form expressions for  $E_1$ ,  $E_2$ , and  $E_3$  have been derived as

$$E_1 = \begin{pmatrix} 16\eta_b^2\mu^4\gamma_b^2\gamma_m^4 + 64\eta_b^2\mu^3\gamma_b^2\gamma_m^3 + 96\eta_b^2\mu^2\gamma_b^2\gamma_m^2 \\ + 64\eta_b^2\mu\gamma_b^2\gamma_m + 16\eta_b^2\gamma_b^2 \\ - 16\eta_b^2\mu^4\gamma_b^2\gamma_m^4 - 64\eta_b^2\mu^3\gamma_b^2\gamma_m^3 - 96\eta_b^2\mu^2\gamma_b^2\gamma_m^2 \\ - 64\eta_b^2\mu\gamma_b^2\gamma_m - 16\eta_b^2\gamma_b^2 \end{pmatrix} \eta_{1,2}^6 + \begin{pmatrix} -16\eta_b^2\mu^4\gamma_b^2\gamma_m^4 - 64\eta_b^2\mu^3\gamma_b^2\gamma_m^3 - 96\eta_b^2\mu^2\gamma_b^2\gamma_m^2 \\ - 64\eta_b^2\mu\gamma_b^2\gamma_m - 16\eta_b^2\gamma_b^2 \end{pmatrix} \eta_{1,2}^4. \quad (127)$$

$$E_2 = \begin{pmatrix} (6\mu^4\gamma_b^2\gamma_m^4 + 24\mu^3\gamma_b^2\gamma_m^3 + 36\mu^2\gamma_b^2\gamma_m^2 + 24\mu\gamma_b^2\gamma_m + 6\gamma_b^2)\eta_{1,2}^8 \\ - 8\eta_b^2\kappa\mu^3\gamma_b^2\gamma_k\gamma_m^3 - 24\eta_b^2\kappa\mu^2\gamma_b^2\gamma_k\gamma_m^2 - 8\eta_b^2\mu^3\gamma_b^2\gamma_m^3 \\ - 8\mu^4\gamma_b^2\gamma_m^4 - 24\eta_b^2\kappa\mu\gamma_b^2\gamma_k\gamma_m - 24\eta_b^2\mu^2\gamma_b^2\gamma_m^2 - 32\mu^3\gamma_b^2\gamma_m^3 \\ - 8\mu^3\gamma_b^2\gamma_m^3 - 8\eta_b^2\kappa\gamma_b^2\gamma_k - 24\eta_b^2\mu\gamma_b^2\gamma_m - 48\mu^2\gamma_b^2\gamma_m^2 \\ - 24\mu^2\gamma_b^2\gamma_m^2 - 8\eta_b^2\gamma_b^2 - 32\mu\gamma_b^2\gamma_m - 24\mu\gamma_b\gamma_m - 8\gamma_b^2 - 8\gamma_b \\ 8\eta_b^4\kappa^2\mu^2\gamma_b^2\gamma_k^2\gamma_m^2 + 16\eta_b^4\kappa^2\mu\gamma_b^2\gamma_k^2\gamma_m + 16\eta_b^4\kappa\mu^2\gamma_b^2\gamma_k\gamma_m^2 \\ + 8\eta_b^4\kappa^2\gamma_b^2\gamma_k^2 + 32\eta_b^4\kappa\mu\gamma_b^2\gamma_k\gamma_m + 8\eta_b^4\mu^2\gamma_b^2\gamma_m^2 \\ + 8\eta_b^2\mu^3\gamma_b^2\gamma_m^3 + 2\mu^4\gamma_b^2\gamma_m^4 + 4\eta_b^2\kappa\mu^2\gamma_b^2\gamma_k\gamma_m^2 + 16\eta_b^4\kappa\gamma_b^2\gamma_k \\ + 16\eta_b^4\mu\gamma_b^2\gamma_m + 24\eta_b^2\kappa\mu\gamma_b^2\gamma_k\gamma_m + 24\eta_b^2\mu^2\gamma_b^2\gamma_m^2 + 8\mu^3\gamma_b^2\gamma_m^3 \\ + 8\eta_b^2\kappa\mu\gamma_b\gamma_k\gamma_m + 4\eta_b^2\mu^2\gamma_b^2\gamma_m^2 + 4\mu^3\gamma_b^2\gamma_m^3 + 8\eta_b^4\gamma_b^2 \\ + 8\eta_b^2\kappa\gamma_b^2\gamma_k + 24\eta_b^2\mu\gamma_b^2\gamma_m + 12\mu^2\gamma_b^2\gamma_m^2 + 4\eta_b^2\kappa\gamma_b\gamma_k \\ + 8\eta_b^2\mu\gamma_b\gamma_m + 12\mu^2\gamma_b\gamma_m^2 + 8\eta_b^2\gamma_b^2 + 2\mu^2\gamma_m^2 + 8\mu^2\gamma_b\gamma_m \\ + 4\eta_b^2\gamma_b + 12\mu\gamma_b\gamma_m + 4\mu\gamma_m + 24\eta_b^2\kappa\mu^2\gamma_b^2\gamma_k\gamma_m^2 \\ + 8\eta_b^2\kappa\mu^3\gamma_b^2\gamma_k\gamma_m^3 + 2\gamma_b^2 + 4\gamma_b + 2 \\ - 8\eta_b^4\kappa^2\mu^2\gamma_b^2\gamma_k^2\gamma_m^2 - 16\eta_b^4\kappa^2\mu\gamma_b^2\gamma_k^2\gamma_m - 16\eta_b^4\kappa\mu^2\gamma_b^2\gamma_k\gamma_m^2 \\ - 8\eta_b^4\kappa^2\gamma_b^2\gamma_k^2 - 32\eta_b^4\kappa\mu\gamma_b^2\gamma_k\gamma_m - 8\eta_b^4\mu^2\gamma_b^2\gamma_m^2 - 16\eta_b^4\kappa\gamma_b^2\gamma_k \\ - 16\eta_b^4\mu\gamma_b^2\gamma_m - 8\eta_b^4\gamma_b^2 \end{pmatrix} \eta_{1,2}^6 + \begin{pmatrix} -8\eta_b^4\kappa^2\mu^2\gamma_b^2\gamma_k^2\gamma_m^2 - 16\eta_b^4\kappa^2\mu\gamma_b^2\gamma_k^2\gamma_m - 16\eta_b^4\kappa\mu^2\gamma_b^2\gamma_k\gamma_m^2 \\ - 8\eta_b^4\kappa^2\gamma_b^2\gamma_k^2 - 32\eta_b^4\kappa\mu\gamma_b^2\gamma_k\gamma_m - 8\eta_b^4\mu^2\gamma_b^2\gamma_m^2 - 16\eta_b^4\kappa\gamma_b^2\gamma_k \\ - 16\eta_b^4\mu\gamma_b^2\gamma_m - 8\eta_b^4\gamma_b^2 \end{pmatrix} \eta_{1,2}^4. \quad (128)$$

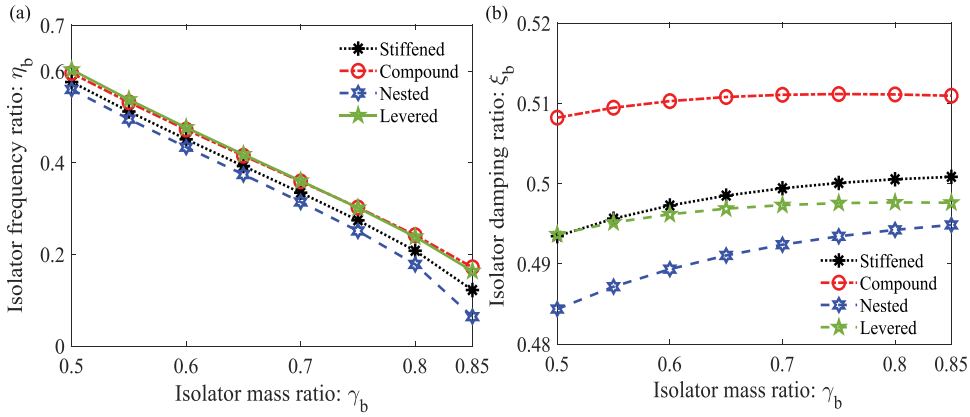


**Figure 18.** The variations of the (a) optimal frequency ratio and (b) optimal damping ratio of stiffened inertial amplifier base isolator, compound stiffened inertial amplifier base isolator, nested stiffened inertial amplifier base isolator, and levered inertial amplifier base isolator. Eqs. (123) and (126) has been applied for these graphs. The values of other system parameters are considered:  $\gamma_k = 0.1$  and  $\nu_a = 0.1$ .

$$E_3 = \frac{2\eta_b^2 \left( -\frac{1}{2} + \left( -\frac{1}{2} + (\mu\gamma_m + 1)\eta_{1,2}^2 + \frac{(-\kappa\gamma_k - 1)\eta_b^2}{2} - \frac{\mu\gamma_m}{2} \right) \gamma_b \right)}{(\kappa\gamma_k + 1)^2 \left( (\eta_{1,2}^2 - 1) \left( (\mu\gamma_m + 1)\eta_{1,2}^2 - \eta_b^2(\kappa\gamma_k + 1) \right) \gamma_b - \eta_{1,2}^2 \right)} \quad (129)$$

Eqs. (123), (124), and the second expression of Eq. (126) have been substituted in the second expression of Eq. (125) to obtain the optimal damping ratio of the isolator.

The variations of the optimal frequency ratio and damping ratio of the stiffened inertial amplifier base isolator, compound stiffened inertial amplifier base isolator, nested stiffened inertial amplifier base isolator, and levered inertial amplifier base isolator have been shown in Fig. 18a,b. According to Fig. 18a, the optimal frequency ratio decreases when the isolator mass ratio increases. In contrast, the optimal damping ratio decreases when the isolator mass ratio increases according to Fig. 18b.

Lower frequency ratio provides higher time period to the isolated structures which helps the main structure to maintain its elastic limit and reduce structural damages during vibration. Higher damping ratio within a certain ranges provides optimal vibration reduction capacity to the isolators. Therefore, a higher isolator mass ratio is recommended to achieve optimum base isolators.

## 6. Dynamic Response Evaluation of the Isolated Structures

To achieve each vibration reduction performance, the single-degree-of-freedom systems are equipped with newly developed base isolators. All isolated SDOF systems have the same governing system parameters.

The  $H_\infty$  optimized design parameters for the conventional and novel base isolators are listed in Table 4 Eq. (3).

The additional tests are carried out to prove the reliability of the proposed methodology in a larger class of seismic excitation scenarios. The Clough-Penzien power spectrum, a modified version of the widely used Kanai-Tajimi spectrum, may be employed as the ground acceleration for this study in order to accomplish this goal. The one-sided PSD that is present in the process sets it apart.

$$\begin{aligned}
X_{\ddot{v}_g} &= S_0 \frac{\omega_f^4 + 4\zeta_f^2 \omega_f^2 \omega^2}{\left(\omega_f^2 - \omega^2\right)^2 + 4\zeta_f^2 \omega_f^2 \omega^2} \frac{\omega_g^4}{\left(\omega_g^2 - \omega^2\right)^2 + 4\zeta_g^2 \omega_g^2 \omega^2} \\
&= S_0 \frac{\omega_f^4 - 4\zeta_f^2 \omega_f^2 q^2}{\left(\omega_f^2 + q^2\right)^2 - 4\zeta_f^2 \omega_f^2 q^2} \frac{q^4}{\left(\omega_g^2 + q^2\right)^2 - 4\zeta_g^2 \omega_g^2 q^2}.
\end{aligned} \tag{130}$$

where the constant power spectral density for random white noise excitation is defined by  $S_0$  and  $q = i\omega$ . The well-known Kanai-Tajimi model's filter parameters are  $\omega_f$  for the soil layer's natural frequency and  $\zeta_f$  for its damping capacity, respectively. A second filter that uses the parameters  $\omega_g$  and  $\zeta_g$  provides a limited power output for the ground displacement. As  $\omega_g \ll \omega_f$ , the second quotient approaches unity very quickly, therefore the second filter only impacts the very low range frequencies. The filter parameter values are obtained from Kiureghian and Neuenhofer (1992) to investigate sites with soils classed as firm, medium, and soft. This study considers soil that is firm.

The structural displacements of the single-degree-of-freedom systems isolated by the  $H_\infty$  optimized base isolators subjected to harmonic and random white excitations have been determined and shown in Fig. 19a,b. According to Fig. 19a, the maximum displacement of the uncontrolled structure has been derived as 50. The maximum displacements of the single-degree-of-freedom systems isolated by the conventional base isolator, stiffened inertial amplifier base isolator, compound stiffened inertial amplifier base isolator, nested stiffened inertial amplifier base isolator, and levered stiffened inertial amplifier base isolator have been determined as 5.2355, 1.9244, 1.9521, 1.9052, and 1.9216. The maximum structural displacement of the novel isolators is compared with the maximum structural displacement of the conventional isolator to obtain the superior vibration reduction capacity of the novel isolators. As a result, the  $H_\infty$  optimized stiffened inertial amplifier base isolator, compound stiffened inertial amplifier base isolator, nested stiffened inertial amplifier base isolator, and levered stiffened inertial amplifier base isolator are 63.24%, 62.71%, 63.60%, and 63.29% superior to the optimum conventional base isolator. According to Fig. 19b, the maximum displacement of the uncontrolled SDOF system under random excitation is evaluated as  $1.4947 \times 10^7$  dB/Hz. The maximum displacements of the SDOF systems isolated by the conventional base isolator, stiffened inertial amplifier base isolator, compound stiffened inertial amplifier base isolator, nested stiffened inertial amplifier base isolator, and levered stiffened inertial amplifier base isolator have been determined as  $5.3703 \times 10^6$  dB/Hz,  $7.7648 \times 10^5$  dB/Hz,  $8.4421 \times 10^5$  dB/Hz,  $7.4631 \times 10^5$  dB/Hz, and  $7.7730 \times 10^5$  dB/Hz. The maximum structural displacement of the novel isolators is compared with the maximum structural displacement of the conventional isolator to obtain the superior vibration

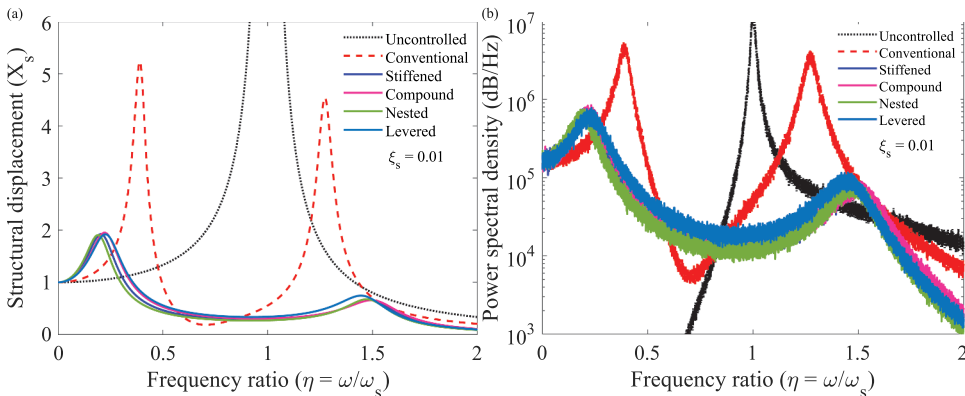


**Figure 19.** The structural displacements of the SDOF systems isolated by the  $H_\infty$  optimized base isolators subjected to (a) harmonic and (b) random white excitations. The structural system parameters of the SDOF systems are considered the same and listed in Table 3.  $H_\infty$  optimized design parameters are listed in Table 4.



**Table 3.** The structural parameter of the SDOF systems.

Primary structure	Governing system parameter	Value
		$\xi_s$
SDOF system	Damping ratio	0.01

**Table 4.**  $H_\infty$  optimized design parameters for the conventional and novel base isolators.

System	Introduced by	$H_\infty$ optimization	
		$\eta_b$	$\xi_b$
Stiffened inertial amplifier base isolator	This study	0.334586	0.49942
Compound stiffened inertial amplifier base isolator	This study	0.359217	0.51107
Nested stiffened inertial amplifier base isolator	This study	0.314332	0.49239
Levered stiffened inertial amplifier base isolator	This study	0.360375	0.497323
Conventional base isolator	Matsagar and Jangid Matsagar and Jangid (2003)	0.50	0.10

Conventional base isolator: isolator mass ratio ( $\gamma_b$ ) = 0.90, stiffened inertial amplifier base isolator:  $\gamma_b = 0.70$ ,  $\phi = 40^\circ$ ; Compound stiffened inertial amplifier base isolator:  $\gamma_b = 0.70$ ,  $\phi = 40^\circ$ ,  $\theta = 64^\circ$ ; Nested stiffened inertial amplifier base isolator:  $\gamma_b = 0.70$ ,  $\phi_1 = 40^\circ$ ,  $\phi_2 = 45^\circ$ ,  $\phi_3 = 45^\circ$ , and Levered stiffened inertial amplifier base isolator:  $\gamma_b = 0.80$ ,  $b_1/a_1 = 1.0$ ,  $b_2/a_2 = 1.0$ . These parameters are applied to the Eq. (123), Eq. (125), and Eq. (126) to obtain each  $H_2$  optimized base isolator's optimal natural frequency and damping ratio.

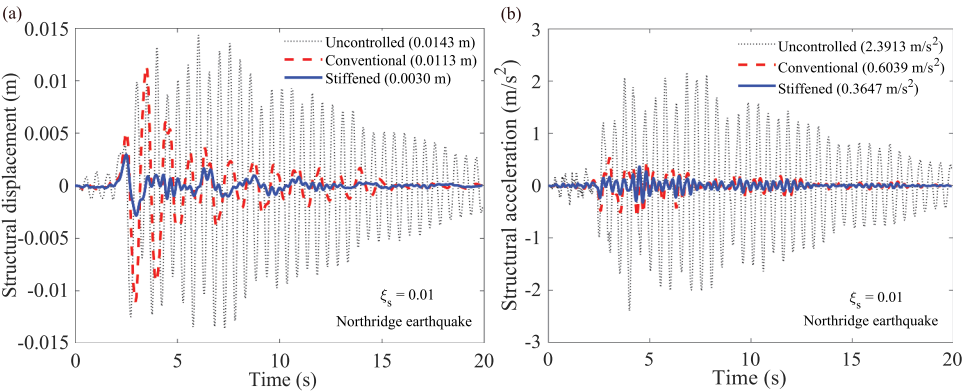


**Figure 20.** The structural displacement and acceleration of the uncontrolled SDOF systems. The responses from the isolated SDOF systems are added in the graphs to project the superior vibration reduction capacity of the stiffened isolators with respect to the conventional isolators. Accordingly, the (a) displacement and (b) acceleration responses of the SDOF systems isolated by the conventional and stiffened isolators are shown in this figure.

reduction capacity of the novel isolators. As a result, the  $H_\infty$  optimized stiffened inertial amplifier base isolator, compound stiffened inertial amplifier base isolator, nested stiffened inertial amplifier base isolator, and levered stiffened inertial amplifier base isolator are 85.54%, 84.28%, 86.10%, and 85.52% superior to the optimum conventional base isolator.

The analytical studies and simulation efforts are also corroborated by a numerical analysis. The Newmark-beta approach is used to do the numerical analysis. This numerical analysis utilizes Northridge near-field earthquake data (pulse) as a loading function. The mass of the major structure is 3000 tons. The structural time period is considered as  $T_s = 0.5$  seconds. The structural period,  $\omega_s = 2\pi/T_s$ , is used to ascertain the natural frequency of the structure. The anticipated viscous damping ratio for the single-degree-of-freedom systems is  $\xi_s = 0.01$ . The displacement and acceleration responses of the single-degree-of-freedom systems isolated by the conventional and stiffened isolators have been shown in Fig. 20a,b.

According to the analysis, the stiffened isolators are 73.98% and 39.62% superior to the conventional isolators in terms of displacement and acceleration reduction capacities. Therefore, the proposed isolators have successfully enhanced the vibration reduction capacity of the conventional isolator effectively by incorporating the amplifiers inside their core materials.

## 7. Conclusions

This paper presented a unified theoretical and analytical framework for designing and evaluating four novel configurations of inertial amplifiers, namely, the conventional, compound, nested, and levered designs, along with their stiffened variants. These amplifiers are integrated into the core materials of the conventional vibration isolators to increase their vibration reduction capacities. These isolators exploit geometrically constrained mechanisms to amplify effective inertia while introducing stiffness tuning elements to control the system's dynamic characteristics. The stiffened versions of each configuration allow independent and simultaneous manipulation of both effective mass and stiffness, enabling broad adaptability to diverse isolation requirements. A key technical advancement of this study is the derivation of closed-form expressions for both mass and stiffness amplification factors as functions of geometric parameters. These expressions were synthesized into a unified frequency tuning relation of the form  $\omega_a = \omega_0 \sqrt{\Lambda_i/\Gamma_i}$ , capturing how the natural frequency of the isolated system shifts with the ratio of stiffness to mass amplification. Inversion formulas were also developed, allowing designers to analytically determine the required stiffness properties to achieve a target frequency shift for a given inertial amplification. This framework eliminates the need for iterative numerical optimization and facilitates transparent and systematic design. Additionally, a comparative analysis was conducted to assess the effectiveness and design trade-offs among the four IA configurations. The nested IA exhibited the highest amplification capacity, while the levered IA offered a more compact design with high scalability. The compound and conventional designs provided intermediate levels of performance with simpler geometries. The performance mapping and parametric studies furnish practical guidelines for implementing these isolators in a variety of structural and mechanical systems. Key novel contributions of this study include:

- Introduction of four novel IA-based passive vibration isolator configurations.
- Development of stiffened variants to enable independent mass and stiffness tuning.
- Derivation of closed-form relations for mass/stiffness amplification and tuning ratio.
- Analytical inversion for stiffness ratio design targeting specific natural frequency shifts.
- Systematic performance comparison to identify optimal configurations for practical use.

These findings mark a substantial advancement in the design of passive vibration isolators by offering enhanced tunability, reduced physical mass, and compact geometric alternatives. The proposed IA-based isolators are especially suited for applications requiring high-performance vibration isolation across a range of frequencies without the need for active components or complex control systems. Future work will aim to explore nonlinear and broadband excitation scenarios and integrate the isolators into multi-degree-of-freedom systems.

## Acknowledgments


The authors would like to acknowledge the post-doctoral grant received from the University of Glasgow during this research work period.

## Disclosure Statement

The authors declare that they have no known competing financial interests or personal relationships that could have appeared to influence the work reported in this paper

## ORCID

Sondipon Adhikari  <http://orcid.org/0000-0003-4181-3457>

Sudip Chowdhury  <http://orcid.org/0000-0001-6218-4843>

## Data Availability Statement

All data, models, and code generated or used during the study appear in the submitted article.

## References

- Acar, G., and C. Yilmaz. 2013. "Experimental and Numerical Evidence for the Existence of Wide and Deep Phononic Gaps Induced by Inertial Amplification in Two-Dimensional Solid Structures." *Journal of Sound and Vibration* 332 (24): 6389–6404. <https://doi.org/10.1016/j.jsv.2013.06.022>.
- Adhikari, S., and A. Banerjee. 2022. "Enhanced Low-Frequency Vibration Energy Harvesting with Inertial Amplifiers." *Journal of Intelligent Material Systems and Structures* 33 (6): 822–838. <https://doi.org/10.1177/1045389X211032281>.
- Alotta, G., and G. Failla. 2021. "Improved Inerter-Based Vibration Absorbers." *International Journal of Mechanical Sciences* 192:106087. <https://doi.org/10.1016/j.ijmecsci.2020.106087>.
- Chen, M. Z., and Y. Hu. 2019a. "Analysis for Inerter-Based Vibration System." *Inerter and Its Application in Vibration Control Systems*, 19–39. Singapore: Springer.
- Chen, M. Z., and Y. Hu. 2019b. *Inerter and Its Application in Vibration Control Systems*. Singapore: Springer.
- Cheng, Z., A. Palermo, Z. Shi, and A. Marzani. 2020. "Enhanced Tuned Mass Damper Using an Inertial Amplification Mechanism." *Journal of Sound and Vibration* 475:115267. <https://doi.org/10.1016/j.jsv.2020.115267>.
- Chowdhury, S., and S. Adhikari. 2025a. "Nonlinear Damping Amplifier Friction Bearings." *Journal of Vibration and Acoustics* 147 (3). <https://doi.org/10.1115/1.4067800>.
- Chowdhury, S., and S. Adhikari. 2025b. "Nonlinear Stiffened Inertial Amplifier Tuned Mass Friction Dampers." *Soil Dynamics and Earthquake Engineering* 191:109264. <https://doi.org/10.1016/j.soildyn.2025.109264>.
- Chowdhury, S., S. Adhikari, and A. Banerjee. 2025. "Advanced Energy Harvesting Vibration Absorbers Using Inertial Amplifiers." *ASCE-ASME Journal of Risk and Uncertainty in Engineering Systems, Part A: Civil Engineering* 11 (3): 04025036. <https://doi.org/10.1061/AJRUA6.RUENG-1529>.
- Chowdhury, S., A. Banerjee, and S. Adhikari. 2021. "Enhanced Seismic Base Isolation Using Inertial Amplifiers." *Structures* 33 (10): 1340–1353. <https://doi.org/10.1016/j.istruc.2021.04.089>.
- Chowdhury, S., A. Banerjee, and S. Adhikari. 2022. "Optimal Negative Stiffness Inertial-Amplifier-Base-Isolators: Exact Closed-Form Expressions." *International Journal of Mechanical Sciences* 218 (3): 107044. <https://doi.org/10.1016/j.ijmecsci.2021.107044>.
- Chowdhury, S., A. Banerjee, and S. Adhikari. 2023. "The Optimal Design of Dynamic Systems with Negative Stiffness Inertial Amplifier Tuned Mass Dampers." *Applied Mathematical Modelling* 114:694–721. <https://doi.org/10.1016/j.apm.2022.10.011>.
- De Domenico, D., G. Ricciardi, and R. Zhang. 2020. "Optimal Design and Seismic Performance of Tuned Fluid Inerter Applied to Structures with Friction Pendulum Isolators." *Soil Dynamics and Earthquake Engineering* 132:106099. <https://doi.org/10.1016/j.soildyn.2020.106099>.
- Den Hartog, J. P. 1985. *Mechanical Vibrations*. Mineola, New York: Dover Publications.
- Di Matteo, A., C. Masnata, and A. Pirrotta. 2019. "Simplified Analytical Solution for the Optimal Design of Tuned Mass Damper Inerter for Base Isolated Structures." *Mechanical Systems and Signal Processing* 134:106337. <https://doi.org/10.1016/j.ymssp.2019.106337>.
- Frandsen, N. M. M., O. R. Bilal, J. S. Jensen, and M. I. Hussein. 2016. "Inertial Amplification of Continuous Structures: Large Band Gaps from Small Masses." *Journal of Applied Physics* 119 (12): 124902. <https://doi.org/10.1063/1.4944429>.
- Giaralis, A., and F. Petrini. 2017. "Wind-Induced Vibration Mitigation in Tall Buildings Using the Tuned Mass-Damper-Inerter." *Journal of Structural Engineering* 143 (9): 04017127. [https://doi.org/10.1061/\(ASCE\)ST.1943-541X.0001863](https://doi.org/10.1061/(ASCE)ST.1943-541X.0001863).
- Goodwin, A. J. H. 1965. Vibration Isolators. Google Patents U.S. Patent No. 3,202,388.
- Howell, L. L. 2001. *Compliant Mechanisms*. 1st ed. New York, USA: Wiley.
- Kiureghian, A. D., and A. Neuenhofer. 1992. "Response Spectrum Method for Multi-Support Seismic Excitations." *Earthquake Engineering & Structural Dynamics* 21 (8): 713–740. <https://doi.org/10.1002/eqe.4290210805>.
- Kuhnert, W. M., P. J. P. Gonçalves, D. F. Ledezma-Ramirez, and M. J. Brennan. 2020. "Inerter-Like Devices Used for Vibration Isolation: A Historical Perspective." *Journal of the Franklin Institute* 358 (1): 1070–1086. <https://doi.org/10.1016/j.franklin.2020.11.007>.
- Lazar, I., S. Neild, and D. Wagg. 2014. "Using an Inerter-Based Device for Structural Vibration Suppression." *Earthquake Engineering & Structural Dynamics* 43 (8): 1129–1147. <https://doi.org/10.1002/eqe.2390>.

- Lazar, I., S. Neild, and D. Wagg. 2016. "Vibration Suppression of Cables Using Tuned Inerter Dampers." *Engineering Structures* 122:62–71. <https://doi.org/10.1016/j.engstruct.2016.04.017>.
- Li, J., and S. Li. 2018. "Generating Ultra Wide Low-Frequency Gap for Transverse Wave Isolation via Inertial Amplification Effects." *Physics Letters A* 382 (5): 241–247. <https://doi.org/10.1016/j.physleta.2017.11.023>.
- Marian, L., and A. Giaralis. 2014. "Optimal Design of a Novel Tuned Mass-Damper-Inerter (Tmd) Passive Vibration Control Configuration for Stochastically Support-Excited Structural Systems." *Probabilistic Engineering Mechanics* 38:156–164. <https://doi.org/10.1016/j.probengmech.2014.03.007>.
- Marian, L., and A. Giaralis. 2017. "The Tuned Mass-Damper-Inerter for Harmonic Vibrations Suppression, Attached Mass Reduction, and Energy Harvesting." *Smart Structures and Systems* 19 (6): 665–678.
- Matsagar, V. A., and R. Jangid. 2003. "Seismic Response of Base-Isolated Structures During Impact with Adjacent Structures." *Engineering Structures* 25 (10): 1311–1323. [https://doi.org/10.1016/S0141-0296\(03\)00081-6](https://doi.org/10.1016/S0141-0296(03)00081-6).
- Neil Sclater, N. C. 2001. *Mechanisms & Mechanical Devices Sourcebook*. 3 ed. New York, USA: McGraw-Hill Professional.
- Orta, A. H., and C. Yilmaz. 2019. "Inertial Amplification Induced Phononic Band Gaps Generated by a Compliant Axial to Rotary Motion Conversion Mechanism." *Journal of Sound and Vibration* 439:329–343. <https://doi.org/10.1016/j.jsv.2018.10.014>.
- Rivin, E. I. 2003. *Passive Vibration Isolation*. ASME Press.
- Smith, M. C. 2002. "Synthesis of Mechanical Networks: The Inerter." *IEEE Transactions on Automatic Control* 47 (10): 1648–1662. <https://doi.org/10.1109/TAC.2002.803532>.
- Smith, M. C. 2020. "The Inerter: A Retrospective." *Annual Review of Control, Robotics, and Autonomous Systems* 3 (1): 361–391. <https://doi.org/10.1146/annurev-control-053018-023917>.
- Taniker, S., and C. Yilmaz. 2017. "Generating Ultra Wide Vibration Stop Bands by a Novel Inertial Amplification Mechanism Topology with Flexure Hinges." *International Journal of Solids and Structures* 106:129–138. <https://doi.org/10.1016/j.ijsolstr.2016.11.026>.
- Wagg, D. J. 2021. "A Review of the Mechanical Inerter: Historical Context, Physical Realisations and Nonlinear Applications." *Nonlinear Dynamics* 104 (1): 1–22. <https://doi.org/10.1007/s11071-021-06303-8>.
- Yilmaz, C., G. M. Hulbert, and N. Kikuchi. 2007. "Phononic Band Gaps Induced by Inertial Amplification in Periodic Media." *Physical Review B* 76 (5): 54309. <https://doi.org/10.1103/PhysRevB.76.054309>.
- Zhao, Z., Q. Chen, R. Zhang, C. Pan, and Y. Jiang. 2019. "Optimal Design of an Inerter Isolation System Considering the Soil Condition." *Engineering Structures* 196:109324. <https://doi.org/10.1016/j.engstruct.2019.109324>.